VibroRegen: Harnessing Vibrational Energy in Suspension Systems for Enhanced Vehicle Efficiency

This project explores the feasibility of enhancing vehicle efficiency by harvesting energy typically lost as heat in traditional suspension systems. Building on the principles of regenerative braking, known to improve efficiency by approximately 6.16%, this work investigates the potential of piezoelectric materials to convert vibrational energy into electrical power. A scaled-down regenerative suspension model was designed, developed, and tested using piezoelectric elements to simulate and analyse energy recovery under varying frequencies and amplitudes representative of real-world driving conditions. Through a combination of physical prototyping and Simulink modelling, the project evaluated power output and efficiency, confirming a quadratic relationship between input force and harvested power. The results support the viability of piezoelectric-based regenerative suspension as a supplementary energy recovery method, offering meaningful implications for the development of more sustainable automotive technologies.

Contents

1. Executive Summary 1
1.1 Aims: 1
1.2 Objectives: 1
2. Literature Review 1
2.1 Introduction 1
2.2 Suspension Systems 2
2.3 Energy Recovery Methods 3
Electrostatic 3
Electromagnetic 4
Piezoelectric 4
Comparisons 5
2.4 Piezoelectric Energy Harvesting 6
Atomic Level 6
2.5 Piezo Materials 7
Natural Materials 7
Ceramic-based Materials 8
Environmental Challenges of PZT 10
Lead-Free Piezoceramics 11
2.6 General performance metrics 12
Compositions of PZT 12
2.7 Piezoelectric Arrangement 14
3. Method 14
3.1 Simulink Model 15
3.2 Physical Model Development 16
System Design 16
Testing set up 22
4. Results 24
4.1 Theoretical – Simulink Model 24
4.2 Practical Testing 27
Voltage-Time Integral Analysis 28

Peak Voltage Analysis 29
Power 31
5. Applicability to Automotive Implementation 33
5.1 Introduction 33
5.2 Power Output and Potential Energy Savings 34
Estimating Scaled Power Output 34
5.3 Cost-Efficiency and Practical Integration 35
Material and Component Costs 35
5.4 Manufacturing and Assembly 35
5.5 Integration into Electrical Architecture 35
5.6 Cost-Benefit Assessment 36
5.7 Conclusion 36
6. Recommendations for Further Work 36
7. Conclusion 37
References 38
Appendices i
Appendix A i
Appendix B iii
Appendix C iv
Appendix D xi

List of Figures:

Figure 1	Undisturbed molecule structure	7
Figure 2	Molecule subject to load	7
Figure 3	Graph depicting the energy consumption in production of piezoelectric materials	12
Figure 4	Graph depicting the toxicology impact in production of piezoelectric materials	12
Figure 5	Graph depicting the eco-indicator of piezoelectric materials	12
Figure 6	Simulink model of the power generation of the system under cyclic loading	16
Figure 7	First prototype design, 1/6th scale model	17
Figure 8	Photo of snapped rod	17
Figure 9	Second prototype design, 1/3rd scale model	18
Figure 10	Third prototype design	18
Figure 11	Final suspension design, with supporting frame	20
Figure 12	Final complete design, with PZT holding system	20
Figure 13	Graph using data collected from Simulink model showing Voltage output against force input at 2.75Hz in one oscillation b	26
Figure 14	Graph using data collected from Simulink model showing power output against force input at 2.75Hz over 10 seconds	26
Figure 15	Graph using data collected from Simulink model showing voltage output against force input at 2.75Hz in one oscillation	27
Figure 16	Graph using data collected from Simulink model showing power output against force input at 2.75Hz over 10 seconds	27
Figure 17	Practical Result: Voltage output against force input at 100mm/min	30
Figure 18	Practical Result: Voltage output against rate of force application reaching 50N	30
Figure 19	Practical Result: Peak positive voltage across all tests, observed at 100mm/min movement speed	31
Figure 20	Practical Result: Graph showing the relationship between energy output per oscillation and force input at 100mm/min	33
Figure 21	Practical Result: Graph showing the relationship between power output per oscillation and force input at 100mm/min	33

List of Tables

Table 1	Piezoelectric Constant of Various Materials	8
Table 2	Piezoelectric Material Properties	9
Table 3	Comparison of Properties of various PZT Compositions	13
Table 4	Practical Test Parameters	23

1. Executive Summary

1.1 Aims:

VibroRegen seeks to investigate innovative approaches to improving vehicle efficiency by examining methods of transforming kinetic energy from suspension vibrations into electrical power. Emphasis is placed on identifying a solution that is efficient, feasible, and cost-effective. Scaled physical models and digital simulations have been used to evaluate energy harvesting capabilities under simulated driving conditions, with the broader goal of contributing to sustainable automotive technology and reducing dependency on fossil fuels.

1.2 Objectives:

- **Develop a Simulation Model**: Create a MATLAB simulation of the suspension system that incorporates the damping coefficient, enabling an assessment of ride comfort across various conditions.
- **Theoretical Power Estimation**: Use the MATLAB simulation to estimate the amount of electrical power that can theoretically be generated from vibrational energy.
- **Prototype Design and Development**: Design and fabricate a scaled prototype of the suspension system to facilitate experimental testing and energy harvesting evaluations.
- **Controlled Testing**: Conduct tests on the prototype under simulated driving conditions by applying controlled vibrations, measuring energy harvesting efficiency across varying frequencies and amplitudes.
- **Performance Analysis and Refinement**: Analyse experimental and simulation data to refine the energy harvesting system, optimising its performance for practical automotive applications.

2. Literature Review

2.1 Introduction

The global shift toward sustainable mobility has catalysed research into innovative methods for energy recovery in vehicles. While regenerative braking has already become a mainstream efficiency-enhancing feature, a vast amount of energy remains untapped within suspension systems, where it is traditionally dissipated as heat. This project investigates the feasibility of a novel energy harvesting approach — using piezoelectric materials integrated within a vehicle's suspension system to convert vibrational kinetic energy into electrical output.

The primary objective was to assess whether a piezoelectric regenerative suspension system can viably support auxiliary vehicle loads or contribute to battery recharging, particularly in hybrid or electric vehicles. Through both theoretical modelling and physical prototyping, the project explores the relationships between key parameters such as force, frequency, and lever ratio, and their impact on power generation efficiency. A MATLAB-Simulink model was developed to predict system behaviour under idealised, resonance-matched conditions, while a scaled physical prototype was constructed to validate these predictions under practical constraints.

Ultimately, the project sought to evaluate the scalability, integration potential and energy savings of such a system when applied to real-world automotive scenarios — laying the groundwork for a supplementary, passive energy recovery technology that operates continuously throughout vehicle motion.

2.2 Suspension Systems

Suspension Systems are integral to vehicle dynamics, safety and comfort, primarily designed to absorb shocks and maintain road contact under varying conditions. They are classified into three categories: passive, semi-active and active systems, each with inherent advantages across ride quality, adaptability and simplicity [1]. Passive systems use fixed damping characteristics, they are very simple and the most cost effect method. Semi-active arrangements feature real-time adjustments for better performance and this adjustability is furthered in active systems which external control units to determine suspension response.

Despite these advancements in performance, a fundamental inefficiency remains. The kinetic energy absorbed by suspension systems is dissipated as heat, leading to substantial energy losses across all vehicle classes.

The suspension system's dissipated energy has been extensively studied. Research estimates that energy dissipation is approximately 80W when city driving in a passenger vehicle [2], reaching up to 400W per vehicle when traveling at 97 km/h on good and average roads [3]. The lost energy increases up to 1kW in Heavy Goods Vehicles (HGVs) at high speeds [3]. Harnessing this otherwise dissipated energy could yield significant improvements in fuel efficiency and emissions reduction. BMW research estimates that a 300W suspension energy recovery system could improve fuel efficiency by 3%, contributing to reduced operating costs and environmental impact [3]. Similarly, Audi AG engineers project that integrating energy-harvesting capabilities into hybrid vehicles could cut CO_2 emissions by 3g/km and enhance economy by 0.7L per 100km [3].

For commercial and freight transport, the financial and environmental benefits are even more pronounced. A study from MIT [4] suggests Wal-Mart could save $13 million annually by deploying regenerative suspension systems across its long-haul truck fleet. This demonstrates the economic viability of this approach for large scale operations. Additionally, aforementioned research indicates that up to 1kW of power could be recovered, this potentially eliminates the need for alternators in heavy-goods and military vehicles [3]. This would result in reduced mechanical load and improved reliability, minimising downtime in industries where consistent function is imperative.

These findings underscore the untapped potential of regenerative suspension systems, reinforcing their role in enhancing vehicle efficiency, reducing emissions and supporting sustainable transport innovation. Through converting previously dissipated energy into usable electrical power, this technology presents a viable, scalable solution for improving energy efficiency across both passenger and commercial vehicle sectors. There are three core kinetic-to-electric transducers that are widely used in energy harvesting: electrostatic, electromagnetic and piezoelectric [5].

2.3 Energy Recovery Methods

Electrostatic

Electrostatic generators operate by utilising the force between charges stored on parallel electrode plates to convert kinetic to electrical energy as these plates are moved by an external load through electric fields [6]. The total output charge is determined by the capacitance of the system, and this can be adjusted through altering the physical distance between the plates or changing the dielectric material used [7]. Furthermore, electrostatic transducers demonstrate higher power densities at smaller scales when compared to electromagnetic alternatives. The difference is due to electrostatic systems scaling between the first and second order of length, whereas electromagnets scale between the third and fourth [6]. The high power-density makes them particularly effective within micro-applications such as MEMS-based transducers. Additionally, these transducers operate at a high-frequency response with a low distortion, enabling precise and low-latency operation [7]. This allows for effectivity in a multitude of systems, making them widely used in applications such as microphones, smoke detectors and printing [8]. Recent developments are expanding their use in ultrasound detection and production [9]. However, unlike electromagnetic and piezoelectric transducers, electrostatic harvesters require an external voltage input, limiting their efficiency in standalone energy-harvesting

applications. Additionally, higher manufacturing costs make them less viable compared to alternative methods [7].

Electromagnetic

Faraday's law of electromagnetic induction outlines how electrical energy is generated when a current carrying conductor moves relative to a magnetic field [10]. In electromagnetic vibration-based power generators, vibration causes the necessary relative movement, inducing an electromotive force (EMF) that drives current flow [11]. The energy conversion can be conducted in two ways, through either linear or rotary systems. Rotary systems are usually more compact and feature a higher power density when compared to the linear counterpart [3]. This, however, comes with the complication of transmissions being necessary, for conversion from vertical displacement into the rotational movement used, inherently imposing losses into the system [3]. The simple structure of linear electromagnetic generators has resulted in extensive research, however geometric restrictions have limited the utility in compact applications. This is furthered by the mass of large magnets negatively impacting automotive applications aimed at improving sustainability

Piezoelectric

Piezoelectric transducers convert mechanical stress into electrical energy by exploiting the piezoelectric effect. This is a phenomenon displayed by non-centrosymmetric crystals where an applied load induces electrical polarisation within the material [12]. The charge difference generates a potential difference across the element, enabling direct mechanical to electrical transduction in a simple, compact and low mass structure [5]. The combination of compactness, high energy density and rapid response time make these materials well-suited for micro-scale applications, with uses in self-powered MEMS sensors and biomedical implants [13]. The positive qualities are furthered by piezoelectric materials being less affected by environmental factors when compared to other transducers, ensuring stable performance in a range of applications [5]. However, their brittleness in bulk piezo-layers and depolarisation over time present durability challenges in prolonged mechanical loading applications [5]. Ongoing research into advanced piezoelectric materials and structural enhancements aims to address these limitations by improving mechanical flexibility, thermal stability and long-term polarisation retention [15]. These developments pave the way for more durable and efficient piezoelectric elements, expanding their viability beyond micro-scale applications but also high-strain and long-duration energy harvesting systems.

Comparisons

Each transduction method harbours advantages and trade-offs, suiting them to different applications based on scalability, efficiency and integration constraints. Electrostatic transducers, while effective in precision applications, such as printers and MEMS devices, present significant limitations for energy harvesting in vehicle suspension. Their requirement for a voltage input, coupled with their generally lower energy density, makes them unsuitable for a self-sustaining regenerative system. However, the power output does not scale down as drastically as electromagnetic transducers which allows them to maintain relatively higher energy densities at very small scales. Despite this, the aforementioned constraints, paired with high manufacturing costs, reduce their viability in the context of mass-produced systems working in automotive applications.

Electromagnetic transducers, which operate using Faraday's Law, provide significantly higher power outputs than comparative electrostatic transducers, with studies showing that HGV applications can recover up to 1 kilowatt [3]. This suggests strong potential for large-scale regenerative suspension systems. However, electromagnetic systems suffer from mass and volume constraints, as necessary large magnets and mechanical transmissions (in rotary designs) lead to weight and geometric challenges in compact suspension systems. Additionally, rotary electromagnetic harvesters, though offering higher power density than linear designs, introduce transmission losses, reducing the overall system efficiency. For this project, these factors limit their suitability as minimising mass and energy losses is a priority for an effective sustainability solution.

Piezoelectric transducers offer the most well-balanced solution for this project, offering direct mechanical to electrical energy conversion without requiring an external power source. They are able to achieve three times greater energy density than both electromagnetic and electrostatic systems [15], making them particularly suited for compact, lightweight and efficient applications. In a mathematical model the PZT bar harvester demonstrated a figure 20x higher than comparable linear electromagnet transducers while still having a smaller size [15]. This suggests, that piezoelectrics are better aligned for functioning within the constraints of a suspension system, where weight efficiency and simple integration are critical. However, brittleness, depolarisation and mechanical fatigue remain key challenges [5], which effects could be accentuated under continuous vibrational loading. Overcoming these issues requires the use of advanced composite materials, improved stress distribution techniques and novel piezoelectric architectures to enhance the durability and maintain long-term energy conversion efficiency.

2.4 Piezoelectric Energy Harvesting

The piezoelectric effect is a property exhibited by certain crystalline materials that allows them to generate an electrical charge when subjected to mechanical stress. This occurs due to the asymmetric distribution of electric dipoles, which shift under strain, inducing a potential difference between the electrodes [16]. The effect was first discovered by Pierre and Jacques Curie in 1880 [11], when they observed that applying mechanical pressure to certain crystals, such as quartz and tourmaline, resulted in electrical polarisation [17]. Since then, this principle has been widely used in energy harvesting, sensing and actuation applications

Atomic Level

Piezoelectricity arises from the structure of non-centrosymmetric crystals, meaning that their internal charge of distribution lacks a centre of symmetry. With no external force applied, the positive and negative charge centres within the crystal coincide, resulting in no net electrical polarisation (Fig. 2.1a). However, when mechanical stress (compression or tension) is applied, the inner structures deform, shifting the charge centres and creating small dipoles (Fig. 2.1b). This atomic change propagates across the material, creating a potential difference that can be harvested into electrical power.

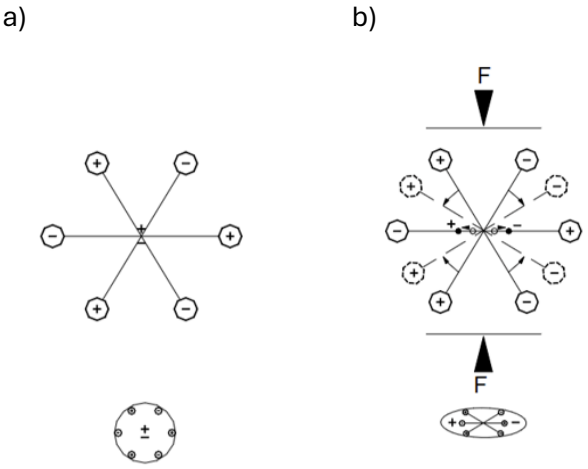

Figure 2.1: Molecular models for visualising a piezoelectric structure a) Undisturbed molecule [16] b) Molecule subject to load [16]

The piezoelectric effect can be categorised into two distinct segments. The direct piezoelectric effect is where a mechanical stress is applied, generating an electrical charge. The direct piezoelectric effect is the foundation of piezoelectric energy harvesting, where mechanical vibrations are converted into usable electricity. Conversely, the inverse piezoelectric effect occurs when an external electrical field is applied to a piezoelectric material, inducing mechanical deformation [17]. The inverse effect is more commonly used in actuators and precision positioning devices.

2.5 Piezo Materials

Piezoelectric materials can be broadly classified into natural, ceramic, polymer and composite materials. The diversity in materials has arisen from over a century of research, with the rate of progress ever increasing.

Natural Materials

Natural piezoelectric materials were the first to be discovered in 1880 [18]. Quartz (SiO_2) was the first discovered piezoelectric material, followed by Rochelle salt, which exhibited a stronger piezoelectric response [19]. While Rochelle salt has a higher piezoelectric coefficient than quartz, its extreme sensitivity to humidity and limited durability prevented its widespread adoption in industrial applications [19]. Instead, quartz became the preferred material due to its high thermal and mechanical stability, making it widely used in precision electronic devices [18]. However, due to its low piezoelectric coefficient, quartz it is not commonly used in energy harvesting applications. Quartz's d_{11} =2.31pC/N is orders of magnitude lower than PZT ceramics (≈ 300pC/N), making it unsuitable for energy harvesting where high charge generation is necessary (Table 2.1). Instead, quartz is widely employed in frequency control, timing application and high precision sensors such as the timing of cardiac cycles and GPS [18]. It is effective within applications where stability and accuracy are prioritised over power output. In piezoelectric strain coefficients denoted as d_{ij}, the first subscript (i) represents the direction of the electric displacement, while the second subscript (j) indicates the direction of the applied mechanical stress. The directional numbers follow a standard convention: 1 and 2 are the plane axis, 3 is the polar axis, and 4–6 refer to shear in each of the planes.

There were limitations in supply of Quartz crystals in the early 20th century as only Brazil produced them, this was a prevalent issue as at this time the allies were utilising quartz crystals in the development of ultrasonic technology to search for U-boats [19]. Natural quartz crystal availability is no longer an issue as all devices are made from artificial crystals in the modern day. This not only mitigates availability problems but also ensures the crystal reaches the required properties to have piezoelectric functionality [18].

While quartz remains indispensable in precision electronics due to its stability and frequency control capabilities, its low piezoelectric coefficient makes it impractical for large-scale energy harvesting applications. As a result, the industry has shifted towards high-performance piezoelectric ceramics and polymers, which offer significantly greater charge generation efficiency for energy recovery systems.

Table 2.1: Piezoelectric Constant of Various Materials [18]

Material	Piezoelectric Constant $d/10^{-12}$ CN^{-1}
Quartz Crystal (SiO_2)	d_{11} = 2.31, d_{14} = 0.727
Lithium Niobate ($LiNbO_3$)	d_{15} = 68, d_{22} = 21
Lithium Tantalate ($LiTaO_3$)	d_{15} = 26, d_{22} = 7
PZT Ceramics ($pb(Zr,Ti)O_3$)	d_{33} = 290-370

Ceramic-based Materials

Ceramic piezoelectric materials, particularly perovskite-structured compounds, have become the dominant choice for energy harvesting applications due to their high charge generation efficiency, tunability and scalability. The development of ceramic materials began from barium titanate ($BaTiO_3$) to lead zirconate titanate ($Pb(Zr,Ti)O_3$) and now to lead free alternatives. The following section explores their properties, manufacturing and advancements, with a focus on their relevance in energy harvesting applications, such as regenerative vehicle suspensions.

In the height of World War 2, researchers in the United States, Japan and Russia sought after materials for compact radar systems that require high-capacitance capacitors [19]. Three materials were tested: $CaTiO_3$, $SrTiO_3$ and $BaTiO_3$. They were chosen due to their perovskite structures, and out of the tested materials the permittivity of barium titanate was found to be enormous comparatively [19].

Limitations prevalent in $BaTiO_3$ such as the large temperature coefficient of electromechanical parameters and aging effect, led researchers to test various ion replacements and dopants [19]. This resulted in the discovery of PZT ($Pb(Zr,Ti)O_3$), which has a significantly higher curie point than $BaTiO_3$ (Table 2.5b), one of the most widely used piezoelectric materials today [20]. A revolutionisation within the field was found when U.S. researchers focused on the morphotropic phase boundary (MPB), where a material is between tetragonal and rhombohedral phases. It was found to be between these phases where ferroelectric materials exhibit significantly higher piezoelectric constants, boosting electromechanical coupling [19]. These findings hugely impacted the ceramic piezoelectric industry, resulting in lead-based ceramics with MBP compositions becoming the standard for high quality piezoelectrics.

The evolution of PZT has been marked by significant advancements in material science, doping modifications and multilayer structuring, ensuring it maintains its stature as the dominant choice for piezoelectric applications. Compared to early piezoelectric ceramics, PZT presents higher charge generation efficiency, electromechanical coupling and increased durability. This allows for

it to be integrated in high performance systems requiring sensors, actuators and energy harvesting.

Studies from 1958, six years after first development of PZT, reported the piezoelectric charge coefficient (d_{33}) for PZT-4 (trademarked by Clevite Corp.) to be 250pC/N, a substantial improvement over $BaTiO_3$ (190pC/N) which was the leading material previously [21]. In comparison, modern PZT-4 has shown an increase to 289pC/N, rising to 593pC/N in PZT-5H™ (Table 2.2), a softer form of PZT, demonstrating the advancements in domain engineering, processing and manufacturing techniques. These improvements have contributed to PZT's continued dominance in modern piezoelectric systems and coined them the name of the "king of piezoelectrics" [22].

Table 2.2: Piezoelectric Material Properties [19, 21]

	Dielectric Const.	Piezoelectric Const. (d_{33}) (10^{-12} C/N)	Curie Point (˚C)
$BaTiO_3$	1700	190	115
$PbTi_{0.45}Zr_{0.55}O_3$	500	130	350
PZT-4™ (1958)	1200	250	340
PZT-4™ (2017)	1300	289	328
PZT-5H™	3400	593	193
Quartz Crystal	4.5	2.3	Not Ferroelectric

Enhancements of PZT

One of the primary factors contributing to the enhanced performance of PZT is the optimisation of the MPB by fine tuning the Zr to Ti ratio in PZT compositions. By altering the ratio of Zr to Ti, the presence of tetragonal and rhombohedral phases varies, and it has been found that between 52.5/47.5 and 55/45 Zr/Ti with the ideal composition altering with processing variations [21]. A further area of improvement is through utilising doping. This allows for many properties, such as mechanical resilience, charge generation and dielectric behaviour of the material, to be fine-tuned for individual applications by introducing particular donor and acceptor dopants. For example, La^{3+} and Nb^{5+} donor doping has been found to enhance electromechanical coupling (k_p = 0.66) and stability. Furthermore, La^{3+} and Fe^{3+} acceptor doping increases the mechanical quality factor (Q_m = 580), improving durability while maintaining efficiency [23]. Through targeted doping strategies, PZT can be optimised for applications ranging from high-sensitivity sensors to high-power generators [24]. A third technique that has been improved upon is the structure of the components. The introduction of multilayered PZT structures significantly enhances the

performance and efficiency of piezoelectric actuators and energy harvesters. By stacking multiple very thin piezoelectric layers, multilayer configurations achieve lower drive voltages [21], reducing power supply costs and improving operational safety. Additionally, the capacitance increases proportionally with the number of layers (n^2 for n layers) [21], leading to lower impedance and improved charge storage, increasing their effectiveness in energy harvesting and actuation. However, these advantages come with challenges in mass implementation. For example, manufacturing costs are higher, both due to complexities in manufacturing as well as the use of rare metals in the necessary electrodes [21]. In addition, in multilayered structures, the mechanical stress of the material is reduced, due to the presence of internal electrodes that cause structural weaknesses under prolonged, cyclical stress. Despite these limitations, multilayer designs remain a crucial innovation, enabling higher energy densities and improved performance. Unfortunately, utilisation of this method will not be undertaken in this project due to budgetary and manufacturing restrictions, however, it remains an area for further development before automotive implementation.

These advancements in composition tuning, doping strategies and multilayer structuring have collectively solidified PZT's position as the dominant piezoelectric material for energy harvesting and actuation. By optimising the material's properties using the various techniques, researchers have significantly enhanced efficiency, durability and adaptability across a wide range of applications. While challenges such as manufacturing complexity, material constraints and costs persist, continued innovations in processing techniques and material engineering are expected to further refine PZT-based technologies, solidifying their applicability in future piezoelectric systems.

Environmental Challenges of PZT

Despite PZT's dominance in piezoelectric applications, its high lead content (~60% by weight [25]) and energy-intensive production present sustainability concerns. This is particularly prevalent in automotive applications, where material sustainability and environmental responsibility are emerging as core factors. One major environmental issue is presented during the manufacturing process of PZT. During sintering and machining, PbO is released, posing risks of environmental contamination and occupational exposure [26]. To address these ecological concerns, EU regulations such as WEEE and RoHS impose strict limits on lead-based electronics, encouraging industries to seek alternative materials [27].

Currently, PZT ceramics cannot be efficiently recycled under conventional waste processing, leading to long-term concerns over PbO leaching in landfills [25]. Furthermore, there are no

established recycling protocols for PZT ceramics, but rising environmental concerns may soon drive the development of regulated disposal and recovery methods [28]. The regulations surrounding lead are very restrictive within the automotive sector. For example, the EU End-of-Life Vehicle (ELV) Directive bans hazardous materials in the production of automotive vehicles, except in cases where no viable alternatives exist. While PZT remains exempt under Appendix II, allowing its continued use in ceramic matrix compounds [29], the long-term sustainability of lead-containing ceramics is uncertain, particularly in industries prioritising eco-friendly practices, such as automotive engineering. Recycling techniques such as oxide-halide perovskite composites have emerged, offering a potentially low-energy method for repurposing waste piezoceramics at only ~1% of the energy cost of new materials [28]. Although lead-free piezoceramics such as KNN and BNT are being developed, they face manufacturing challenges and environmental trade-offs. These include high processing energy and difficulties in achieved the necessary fine-grained microstructures in large-scale production [27].

Lead-Free Piezoceramics

A focal point of current research is the development of lead-free piezoceramics. Bismuth sodium titanate (BNT) and potassium sodium niobate (KNN) are two current forerunners to replace lead-based piezoelectrics, due to their appealing properties [27]. They stand far ahead of other lead-free ceramics ($LiNbO_3$ and $BaTiO_3$ for instance) when regarding their piezoelectric effect, relative costs in fabrication and crystallographic symmetry [27]. KNN, in particular, features a high piezoelectric constant, a high Curie temperature and compatibility with low-cost nickel electrodes, making it a highly prospective material [27]. BNT, on the other hand, requires complex uncommon metallisation, increasing the materials cost of production [27]. However, when evaluating the entire life cycle of these potential replacements of PZT it is clear to see that although the toxicity is eliminated, there are still clear limitations in sustainability that need to be addressed (Figure 3, 4). The negative impact of KNN across energy consumption and toxicology impact originate from the presence of niobium, implementing difficulties in extraction and manufacturing [27]. As for BNT, although it appears to possess an environmental improvement over PZT, 90-95% of bismuth produced through lead smelting diminishes any advancement [30].

Although there are currently no viable lead-free materials to fulfil the role of PZT, regulatory pressure and sustainability concerns necessitate ongoing research into this field. Future progress will depend on advancements in material composition, energy efficient fabrication techniques and recycling solutions to guarantee the long-term sustainability of effective piezoceramics.

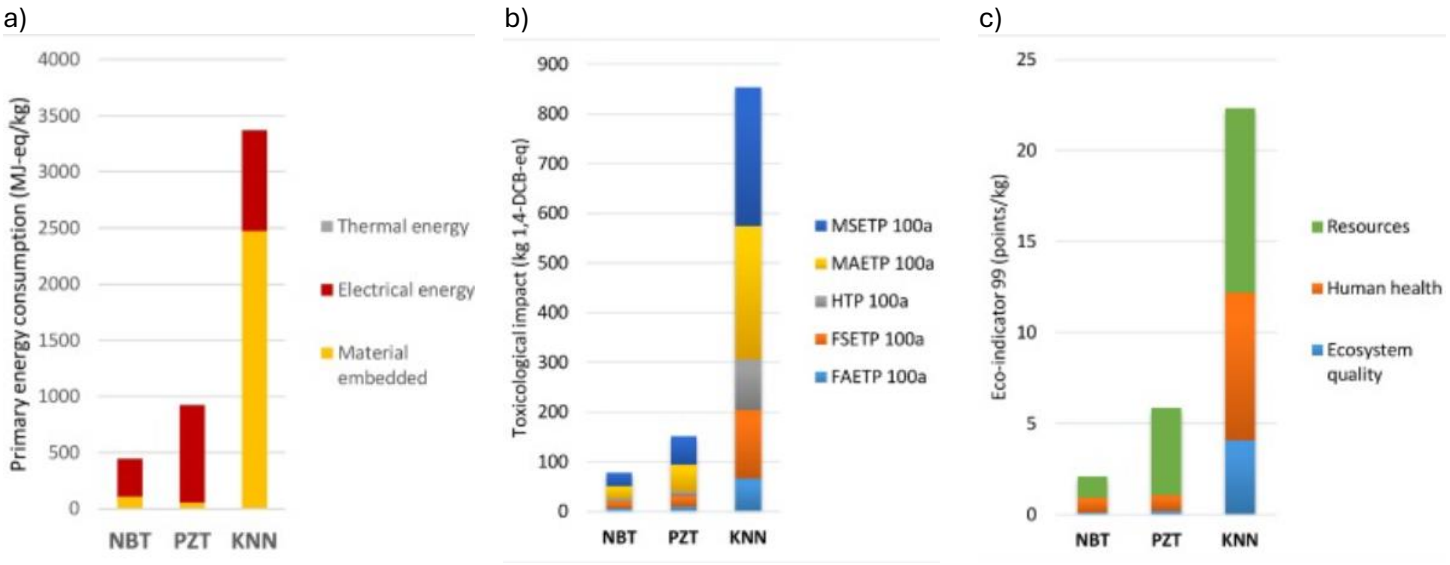

Figure 2.2: Key graphs depicting the environmental impact of piezoelectric materials a) Energy consumption in production [30] b) Toxicology impact of the material [30] c) Eco-indicator of each material

2.6 General performance metrics

In selecting the optimal PZT composition for regenerative suspension applications, several key metrics must be considered. These are crucial to ensure high energy conversion efficiency, durability and thermal stability while maintaining cost and integration practicality.

The following five parameters are essential in evaluating piezoelectric materials for effectivity in energy harvesting within suspension systems. Firstly, the electromechanical coupling factor (k) represents the efficiency of converting mechanical energy into electrical energy. The piezoelectric and voltage coefficients (d_{33}, g_{33}) relate to the charge and voltage generated per unit force applied. Higher k and d_{33} values represent greater harvesting efficiency, making them key characteristics of an effective transducer. Two important characteristics for application within an automotive system, specifically within the suspension, are the mechanical quality factor (Q_m) and the Curie temperature (T_C). The material durability and resistance to mechanical energy losses is represented by Q_m, and the maximum temperature before piezoelectric properties are loss is T_C. Finally, the dielectric loss (tanδ) measures the energy dissipated from the material as heat, meaning lower values relate to an overall higher efficiency.

Compositions of PZT

Due to the aforementioned challenges with the various materials explored, from early PZT predecessors like $BaTiO_3$ to extensively researched lead-free alternatives, I have chosen to utilise PZT for this project. However, even within PZT-based materials, multiple compositions exist, each with distinct properties necessitating a comparison between PZT-5H, PZT-4, and PZT-8 to determine the most suitable option.

PZT-5H demonstrates the highest k (0.75) and d_{33} (593x10^{-12}m/V) values (table 2.3), making it the most efficient at converting mechanical stress into electrical charge, crucial for maximising power harvesting. In contrast, PZT-4 and PZT-8 exhibit significantly lower d_{33} values, under half of PZT-5H, with PZT-8 showing the lowest.

However, while PZT-5H offers superior energy conversion efficiency, it has a low mechanical quality factor (Q_m=65). This suggests reduced durability under prolonged cyclic loading, a critical factor in suspension application, where continuous vibrations and stress are present. Conversely, PZT-8 has the highest Q_m (1000), making it the most resistant to mechanical stresses, ideal where longevity and stability are prioritised. PZT-4 (Q_m=500) sits between these extremes, offering a balance between energy efficiency and durability.

A key consideration for automotive applications is the temperature range the material must be effective within. This is due to suspension systems being exposed to fluctuating temperatures in varying climates and driving conditions. PZT-8 (T_C=300˚C) and PZT-4 (TC=325˚C) are well suited to this application, with their temperatures being far higher than what would be expected, meaning that no noticeable transduction efficiency should be present within operating temperatures. PZT-5H, however, has a T_C of 193˚C limiting its effectivity in dynamic automotive applications where heating from the environment, and the vehicle itself, will be present, impacting the performance of the system. Dielectric loss (tanδ) represents the proportion of energy dissipated as heat from the material and this value is highest in PZT-5H (2.00%), with both PZT-4 and PZT-8 being drastically lower (0.40%).

A comparison of these parameters has brought me to the decision of utilising a material with properties as similar to PZT-4 as possible for this project, dependant on budget and availability in low quantities. This will best reflect the necessary properties for wide-scale implementation into the automotive industry, this material choice is reflected in similar research [15, 31].

Table 2.3: Comparison of Properties of various PZT Compositions [19]

	PZT-5H	PZT-4	PZT-8
Dielectric Const., k	0.65	0.58	0.51
Piezoelectric Coeff., d_{33} (10^{-12}m/V)	593	285	225
Voltage Coeff., g_{33} (10^{-3} Vm/N)	19.7	24.9	25.4
Quality Factor, Q_m	65	500	1000
Cure Temp., T_C (˚C)	193	325	300
Dielectric Loss Tangeant, Tanδ (%)	2.00	0.40	0.40

2.7 Piezoelectric Arrangement

The arrangement of piezoelectric (PZT) elements significantly impacts energy conversion, mechanical durability and electrical impedance in regenerative systems.

A stacked PZT configuration increases voltage output by aligning multiple layers in series, but this comes at the cost of higher stiffness, reducing strain-induced charge generation. Additionally, stacked arrangements exhibit higher impedance, which limits efficient power transfer, particularly at low-frequency vibrations typical in automotive suspension systems. Furthermore, stress concentration in stacked layers increases the risk of mechanical failure, making them less durable for continuous vibrations in vehicle suspensions. The increased material stress also requires higher-grade, mechanically robust PZT materials, which increases manufacturing costs.

In contrast, a parallel PZT configuration allows greater mechanical deformation, leading to high charge generation per cycle and better mechanical resilience by distributing stress more evenly. Parallel arrangements also lower electrical impedance, enabling better power transfer efficiency and reducing energy losses when interfacing with wider circuits. Although parallel configurations generate lower voltage, they produce higher current, which is easier to step up using automotive power electronics.

Given these advantages, a parallel PZT configuration was chosen for this project. It provides higher energy output consistency, improved mechanical durability, lower impedance for efficient energy transfer and reduced material costs. These properties ensure a practical and scalable solution for automotive regenerative systems.

3. Method

The development of this piezoelectric regenerative suspension system involved two complementary approaches: a physical prototype and a Simulink simulation model. The combination of these methods was essential to evaluate the system's feasibility and efficiency in both practical and theoretical contexts.

The Simulink model provides a controlled simulation to assess the feasibility of this system. It enables testing of various parameters pertaining to design parameters and material choices, giving the opportunity to make better informed decisions before creating the physical model. Furthermore, it will act as a benchmark to compare experimental results against, quantifying deviations due to manufacturing tolerances, material inconsistencies and real world inefficiencies.

The physical model will provide essential validation, ensuring that the design can be successfully manufactured and assembled while identifying real-world limitations, such as material constraints, mechanical losses and variations in force distribution. Through experimental testing, the physical model provides insight into actual system behaviour, reflective of how the system would act when integrated within a vehicle. This dual approach ensures a comprehensive evaluation, bridging the gap between theoretical predictions and practical implementation.

3.1 Simulink Model

Given the complexity of interactions within the piezoelectric regenerative suspension system, particularly regarding force application profiles and piezoelectric properties, a Simulink model was critical. Utilising the model allowed systematic isolation and precise adjustment of each of these variables to understand their individual and combined effects on voltage generation and overall system efficiency.

Parameters used in Simulink Model

Typical road conditions encountered when driving passenger vehicles induce vibrational frequencies ranging between 1 and 10 Hz throughout the vehicle due to road irregularities and surface conditions. However, for accurately simulating the load profile specifically acting upon the piezoelectric elements, the frequency range of 1.5 to 4 Hz is most relevant [32] (table 3.2). This range represents the typical vertical motion of the sprung mass, directly influencing suspension compression and thus generating the mechanical load applied to the PZT. While higher frequencies reaching 10 Hz are relevant to the unsprung mass, this does not relate to the load applied to the suspension system itself and therefore does not affect the voltage output.

To determine the amplitude of the applied vibration, the kerb weights of some of the best-selling hybrid vehicles, namely the Toyota Prius, Toyota RAV4 and Honda CR-V, were evaluated. These vehicles exhibited kerb weights ranging from approximately 1375 to 1822 kg [33, 34, 35], resulting in an average kerb weight estimation of 1600kg. Assuming approximately 85% of the total mass is sprung mass, this yields a sprung mass of 340kg per corner, equivalent to a load of 3335N. For the 1/3 scaled model, the load was scaled by a factor of 1/27, resulting in an input amplitude of approximately 120N, representing a mass equivalent of 12.6kg. These results are used in the Simulink models represented in Figure 3.1 and Appendix A, ensuring the simulation realistically reflect vehicle conditions at the appropriate scale.

The lever ratio (LR) variable is varied between 0.5 and 2 to ensure that the highest possible force is applied to the PZT elements without exceeding the 15N operational limit they are rated to. To

reach this optimal force, the output load from the lever should reach a maximum value of 60N to optimise energy harvesting capabilities while maintaining the operational integrity.

Additionally, the simulation utilised electrical properties of the piezoelectric elements, including the dielectric constant (D33) and the capacitance (C). The dielectric constant chosen (255×10^{-12}) is the midpoint between the values for PZT-4 and PZT-8 (shown in table 2.3) as the chosen PZT elements for this test hold various very similar properties to both. The capacitance (0.9×10^{-9} F) is given on the piezoelectric elements datasheet, and this determines the electrical response of each element. These values are crucial in calculating the voltage output in Figure 3.1.

The Simulink model developed specifically for accurately evaluating the power generating potential of the regenerative suspension system is illustrated in Figure 3.1, with corresponding tables of variable definitions, individual block descriptions and MATLAB script used for numerical analysis and result processing is included in Appendix A. Additionally, a complementary Simulink model representing the suspension movement dynamics is also provided in Appendix A. Although not directly necessary for power output simulation, it serves as a valuable reference tool for testing suspension performance parameters.

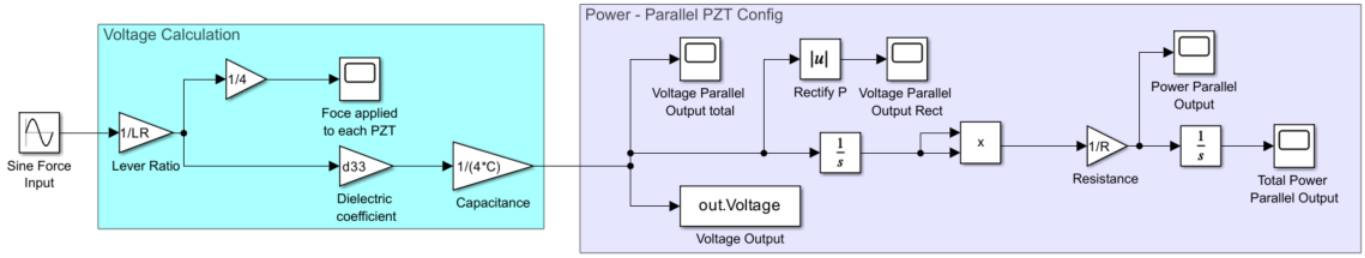

Figure 3.1: Simulink model of the power generation of the system under cyclic loading

3.2 Physical Model Development

System Design

Suspension System Design

The initial plan was to construct a 1/6th scale model of the model to balance size, cost and manufacturability. A full-scale model was financially unfeasible within this project due to the high cost of frame materials and piezoelectric components (PZT). Additionally, a smaller-scale system simplified manufacturing and testing, applying lower scaled forces, allows for PolyLactic Acid (PLA) to be used in the structure giving the possibility for 3D-printing to be the chosen manufacturing method. This reduces complexity, cost and material waste over other methods, using CNC milling and aluminium for example

However, upon printing the first prototype (Fig. 3.2a), it became evident that this scale posed significant manufacturing and testing complexities. The small size resulted in difficulties in machining and assembly, particularly for thinner components such as the rods and the lever (Fig. 3.2b). This was compounded by 3D-printing inaccuracies being proportionally amplified at this scale, compromising the fitment, structural integrity and overall reliability, making it unsuitable for effective testing.

To address these issues, the model scale was increased to 1/3rd, providing a more practical size while still maintaining it is within a feasible budget. This adjustment improved fabrication accuracy, component strength and facilitated easier assembly. This change improves the reliability of testing, as well as making the prototype more representative of a full-scale model which allows for better validation of performance and energy harvesting efficiency.

a) b)

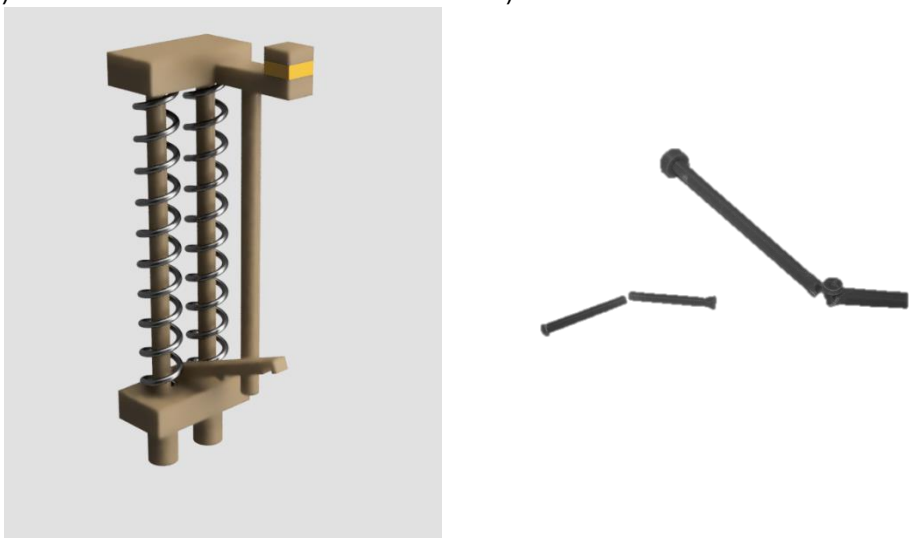

Figure 3.2: a) First prototype design, 1/6th scale model b) Photo of snapped rod.

Following the limitations identified in the initial prototype, a second iteration of the design was developed with a focus on modularity and improved strength, as shown in Figure 3.3a. The model was scaled up to 1/3, allowing for significantly thicker components and improved structural strength. The design was also improved in its modularity, with rods and plates fitting together using slot-in connections, allowing for easier assembly and part replacement. Critical load-bearing sections, particularly the lever and frame, were thickened to prevent mechanical failure during testing. While this improved version performed successfully during initial trials weaknesses remained, most notably in the rod holding attaching the lever pivot to the structure. Additionally, after discussions regarding the available tensile testing machines, it was found that the design was required to be inverted vertically, necessitating a redesign.

These necessary changes were introduced in the third design, refining structural and functional properties of the system shown in Figure 3.3b. Most notably, the lever support structure was relocated externally, independent from the main suspension body. This change ensured greater stability and eliminated lateral loading on the system during operation. Additionally, the lever was now secured to the support using a central pin, providing a fixed axis of rotation rather than relying on resting upon a pivot as in the previous versions. In line with the requirements of the tensile testing apparatus, the spring assembly was flipped, enabling correct load alignment. While these modifications resolved earlier issues related to strength and alignment, new complications emerged. The external lever frame, though structurally rigid, became unstable due to its tall height and narrow base, leading to tipping under load. More critically, during testing with the elastic band in place, it became apparent that the levers movement was impaired. Because the lever rested atop the spring's moving platform, there was no mechanism to pull it downward against the elastic band. This resulted in compressive force not being sufficiently transferred to the PZT elements, compromising the system's energy harvesting functionality.

a) b)

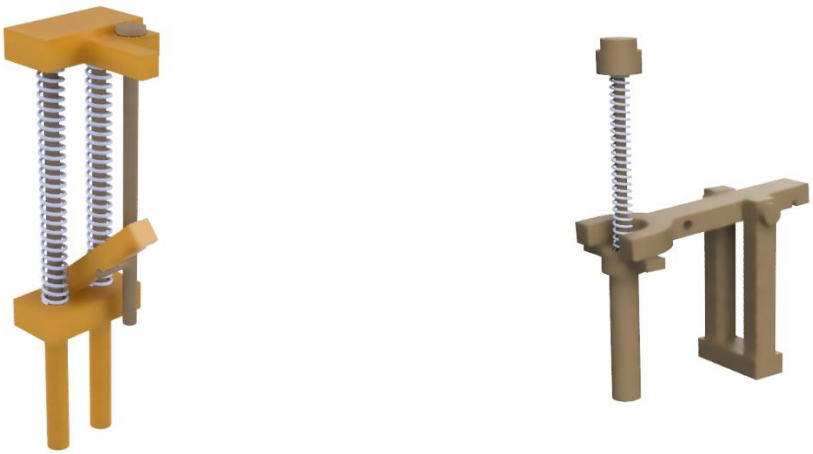

Figure 3.3: a) Second prototype design, 1/3rd scale model b) Third prototype design

To resolve the lateral instability encountered in previous prototypes, the spring structure was reinforced with a supporting external frame that encased the spring and held it in vertical alignment throughout the loading process. A dedicated spring holder was introduced, secured using M3 nuts and bolts, which clamped the top of the frame around the spring housing and prevented deflection or misalignment under compressive force shown in Figure 3.4a. These additions ensured that the spring could undergo axial compression without shifting, significantly improving system reliability and reducing the risk of structural failure.

The lever underwent substantial redesign to address previous issues with ineffective motion and instability. A slot was incorporated into the lever body, allowing it to consistently connect to the spring housing. This ensured that force could be applied from both above and below without the lever rotating or slipping laterally, preserving consistent contact with the elastic band. Multiple mounting holes were added along the lever to enable testing of different lever ratios, offering experimental flexibility in adjusting force amplification. Unlike earlier versions that rested passively on a pivot, the lever in the final design was securely pinned through its centre, maintaining a fixed rotation axis and eliminating any play in its motion.

To eliminate the tipping and flexing seen in prior designs, the lever frame base was significantly enlarged and redesigned to fit securely around the PZT holder. The redesign not only increased the contact area with the underlying structure but also anchored the frame more effectively, preventing movement during force application. The wider base provided a low centre of gravity, enhancing the system's stability when subjected to vertical loads.

The piezoelectric element holder was redesigned with slots to accommodate four PZT discs, holding each securely in place while ensuring equal spacing and load distribution. To simplify wiring and prevent obstruction, dedicated holes were included in the holder's walls for the wires to exit. This improved the functionality while reducing the risk of electrical shorts or interference.

Together, these refinements produced a robust and modular final design that successfully balanced structural stability, experimental flexibility and functional performance, shown in Figure 3.4b. This allowed reliable testing and accurate measurement of piezoelectric energy output under dynamic loading conditions.

a)

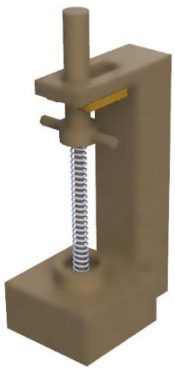

b)

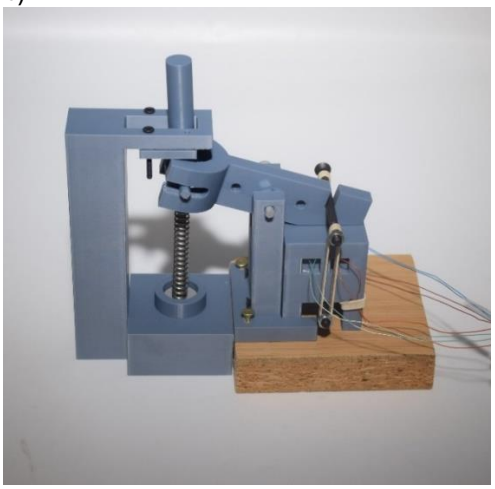

Figure 3.4: a) Final suspension design, with supporting frame b) Final complete design, with PZT holding system

Elastic Band

The elastic bands in the suspension system serve two critical roles: progressive force application on the piezoelectric (PZT) elements and secondary damping to manage vibrational energy. Unlike a rigid mounting system, the elastic band allows the force exerted on the PZT elements to increase gradually. This ensures that excessive stress and sudden force spikes do not reduce efficiency or cause material fatigue. Additionally, in extreme cases where excessive force is applied, the elastic bands are designed to snap first, preventing costly damage to the PZT and minimising repair costs.

Since the PZT is only loaded by the elastic band, the force applied to the PZT is purely from the elastic bands' restoring force. This is shown in equation 3.1, where F_{PZT} is the force directly applied to the piezoelectric element, while F_{lever} represents the force transmitted through the mechanical lever. The lever's restoring motion is governed by the elastic band, modelled as a linear spring with stiffness k_e, where x is the band's elongation from its rest position, determining the magnitude of the restoring force via Hooke's Law ($F = k_e \cdot x$).

$$F_{PZT} = k_e x = k_e \frac{F_{lever}}{k_e}$$

Equation 3.1

Beyond force transfer, the elastic band introduces damping, which helps to smooth vibrations. This damping force is given in equation 3.2, where c_e is the damping coefficient of elastic band (Ns/m) and $\dot{x}$ is the velocity of suspension displacement (m/s):

$$F_{damping} = c_e \dot{x}$$

Equation 3.2

By absorbing sudden impacts and reducing high-frequency oscillations, the elastic band improves system stability and longevity while maintaining effective energy harvesting.

PZT

The selection of a suitable piezoelectric (PZT) element is critical in the design of an efficient regenerative suspension system. Specifically, a material exhibiting properties intermediate between PZT-4 and PZT-8 was desired, balancing dielectric efficiency and mechanical strength. This ensures that the PZT elements maintain high energy conversion efficiency, while also providing sufficient structural integrity to withstand the repeated and variable loading conditions inherent in automotive suspension environments.

Components with titanium cymbals atop a square PZT piezoceramic were selected due to their simple geometry, facilitating straightforward soldering on the contact pads and ease of integration within the mechanical structure of the system. The shape is practical allowing for uniform force

distribution and efficient electrical connectivity, which simplifies both manufacturing and future maintenance operations.

Cost-efficiency was a significant factor influencing material choice, aligning with project budget constraints. Consequently, the TDK PowerHap Piezo Haptic Actuator (model: B54102H1020A001) was chosen due to its balance of performance and affordability. The TDK PowerHap offers a large displacement of up to 65µm, a force capacity of 15N per element, rapid response times and a wide range for the operating temperature, from -40˚C to +85˚C [36]. These properties result in a durable and efficient piezoelectric element, ensuring application in automotive systems is effective.

PZT Arrangement

A parallel configuration of four PZT elements was implemented, due to the benefits over a series arrangement given in section 2.7. A parallel configuration introduces higher capacitance, beneficial in energy harvesting contexts as it enhances the overall electrical energy storage capacity and reduces the resistance of the system. Research highlights this improvement of efficiency, with parallel arrangements outputting far higher power over series (7.676mW compared to 1.671mW respectively [37]) under similar vibrational electromechanical transduction. Such results reinforce the selection of a parallel configuration for achieving optimal energy harvesting capabilities.

Load Distribution Mechanism

To further ensure reliability and uniform distribution across all PZT elements, a dedicated load-distributing block was implemented. This block uniformly transmits the mechanical forces across each PZT element, ensuring balanced mechanical loading and optimal operation. A central supporting rod that travels through the block guarantees precise positioning and orientation, crucial for achieving maximum efficiency and minimising the potential for uneven stress concentrations or overloading.

Lever

By utilising a lever system within my design, it is possible to vary the force applied to the PZT without changing the load onto the suspension system, shown in equation 3.3. The lever either amplifies force while reducing displacement or increases displacement while reducing force depending on the chosen ratio. This is a key feature of the system as it ensures that the force is sufficient for effective energy conversion while not overloading the PZT, preventing mechanical

failure. To provide optimisation for different loads, it is possible to vary the lever ratio used in this system between 0.5 to 2.

$$F_{PZT} = \frac{F_{suspension}}{lever\ ratio}$$

Equation 3.3

A high lever ratio ($r_{lever} > 2$) would increase PZT displacement, which is ideal for flexible, low-stiffness energy harvesting materials. However, since PZT elements are inherently stiff, excessive displacement could lead to mechanical instability. A low lever ratio ($r_{lever} < 0.5$) would amplify the force, but risks resulting in inefficient charge generation due to exceeding the material's strain limits. Thus, a moderate lever ratio was selected to balance force and displacement.

Testing set up

Mechanical Set Up

The primary objective of mechanical testing is to evaluate the PZT's voltage response under a controlled force application. The H1KS 1kN Benchtop tensile tester [38] was used to precisely apply force to simulate a single oscillation of a vehicle's suspension system. The test setup enables variation of both the maximum force magnitude and the speed of loading, ensuring a comprehensive assessment of the system's response over varying situations.

The force applied throughout the testing is within the range of 15-80N (Table 3.1). This range is chosen to ensure system stability and structural integrity. This is crucial considering that PLA is the primary material of the structure, therefore the force range ensures the system remains functional without excessive stress that could lead to mechanical failure. While the theoretical model utilises higher forces, practical constraints required modifications to ensure durability and consistency during testing. To compensate for the difference between the theoretical force predictions and practical material limitations, the lever ratio will be halved ($r_{lever} = 1$) to guarantee the force applied is consistent with that of the theoretical predictions. Using a lever ratio of 1 results in the load from the lever being varied between 15-80N from the H1KS in the practical test, and the theoretical scaled force from an average hybrid vehicle being 75N. Closely matching these force ensures that experimental results remain relevant, valid and directly comparable to the theoretical model. The speed range of 30-100mm/min (table 4) represents different rates of force application, simulating both gradual suspension compression (for example road undulations) and sudden impacts (such as potholes). By varying the velocity of movement, it is possible the analyse how the voltage output fluctuates over different loading conditions as would be present if implemented within a vehicle.

Table 3.1: Practical Test Parameters

Test Parameters	**Values**
Force range	15-80N
Speed of load application	30-100mm/minute
Speed of retraction	250mm/minute
Load Profile	Increasing force as machine clamps

Electrical Set Up

To accurately record the PZT's voltage response, a Tektronix MSO 2024B oscilloscope was used. The oscilloscope records the voltage output of the PZT over time, producing high-resolution data that were processed in MATLAB. The Tektronix oscilloscope was selected due to its 1GS/s sampling rate and very high record length (1M points) [39]. This precise resolution will allow for precise post-processing of the results, giving a better opportunity to identify noise and understand slight changes throughout the force application. MATLAB was used to extract key voltage characteristics, such as total voltage output, peak-to-peak values and the effect of load profiles on voltage response. The data processing will allow for validation of theoretical predictions against experimental results.

Experimental Setup – Practical Considerations

The PZT elements are tested within the entirety of the system (shown in Figure X) rather in isolation to ensure an accurate representation of real operational conditions. The components of the system are joined through pinning, nuts and bolts, screws and adhesive where appropriate. Furthermore, a clamp is used to ensure a strong join to the base of the testing rig. The secure fitment of different components ensures reliability in functionality and results. When implemented into a vehicle, the regenerative unit will be secured to the subframe in a manner consistent with the experimental setup. Between each test the rigidity and positioning of the system is checked to ensure structural integrity and that the load is applied at the intended point.

Expected Outcomes and Performance Metrics

The success of the test was determined by two key metrics, the voltage (and therefore power) output response and the consistency of results. These two key performance indicators serve as a measure of success across the entire system, encompassing every stage from design and material selection to manufacturing, electronic assembly and integration.

A high voltage output indicates that the mechanical design effectively transfers force to the PZT elements, ensuring optimal strain for charge generation. This reflects successful design choices, such as the PZT composition and arrangement, the lever ratio and elastic band stiffness, to maximise energy harvesting. Similarly, consistent results across multiple tests confirm the precision of the manufacturing process, the strength of the design and stability during loading.

Together, these metrics provide a holistic assessment of system performance, demonstrating whether the theoretical design translates successfully into a functional, real-world energy harvesting system.

4. Results

4.1 Theoretical – Simulink Model

An analysis of results from the piezoelectric regenerative system modelled in Simulink follows. The data collected focuses on key relationships between input force, frequency of loading, lever ratio and output power/voltage.

Effect of Input Force on Power Output

Figures 4.1a and 4.1b graph the relationship of input force and power output under consistent conditions. The system was simulated with a lever ratio of 1 and a constant load frequency of 2.75Hz. Figure 4.1a presents the power output per oscillation, showing the instantaneous output, and Figure 4.1b illustrates the cumulative power output over a 10 second period, reflecting realistic extended performance. Both figures fit quadratic equations, showing the nonlinearity of the system's power response to input force.

The fitted equation for an individual cycle's power output (Figure 4.1a) is represented by equation 4.1, where P is the power output and F is the force input.

$$P = 2 \times 10^{-5}F^2 - 3 \times 10^{-7}F + 6 \times 10^{-6}$$

Equation 4.1

The dominant squared coefficient emphasises the quadratic relationship and largely determines the shape of the results. This behaviour aligns with the theoretical model shown in Equation 4.3, therefore validating the model used to simulate the system. This confirms that the power output from the piezoelectric elements is proportional to the square of the applied force.

The small linear term ($-3 \times 10^{-7}F$) and minor negative offset (6×10^{-6}) in the best fit equation are attributed to simulation precision limits, rounding disparities and, primarily, the lack of real-

world system losses. This shows that even in idealised simulations, subtle numerical fluctuations during data capture can result in very small offsets from ideal results.

However, these terms do not meaningfully affect the overall trend, which remains consistent with theoretical expectations. The strong match between the simulations output and the derived equation reinforces the validity of the model and confirms that higher forces yield disproportionately greater power outputs.

The equation relating the force input to the power output over 10 seconds, visualised in Figure 4.1b, is shown in equation 4.2.

$$P = 0.0005F^2 + 1 \times 10^{-6}F + 2 \times 10^{-6}$$

Equation 4.2

Equation 4.2 retains the same quadratic form as the individual cycle model (equation 4.1), but with a significantly larger squared coefficient. This reflects the amplifying effect of an extended time period, allowing a large quantity of oscillations to occur. As a result, the system generates 1.6W with an input force of 60N in 10 seconds.

The slightly negative linear term and small offset once again stem from ideal simulation conditions with negligible data collection differences. However, the curve remains upwardly quadratic and consistent with the theoretical model. This reinforces the idea that real-world applications utilising road vibrations can produce substantial cumulative energy outputs.

a)

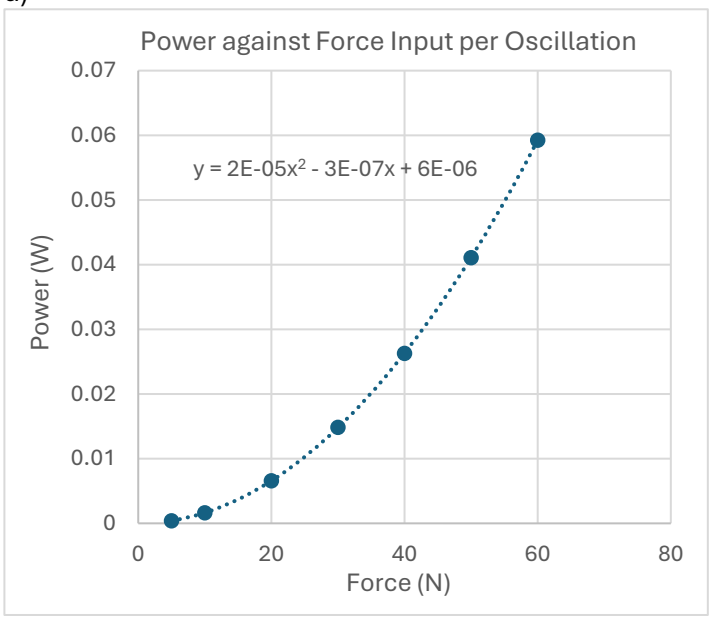

b)

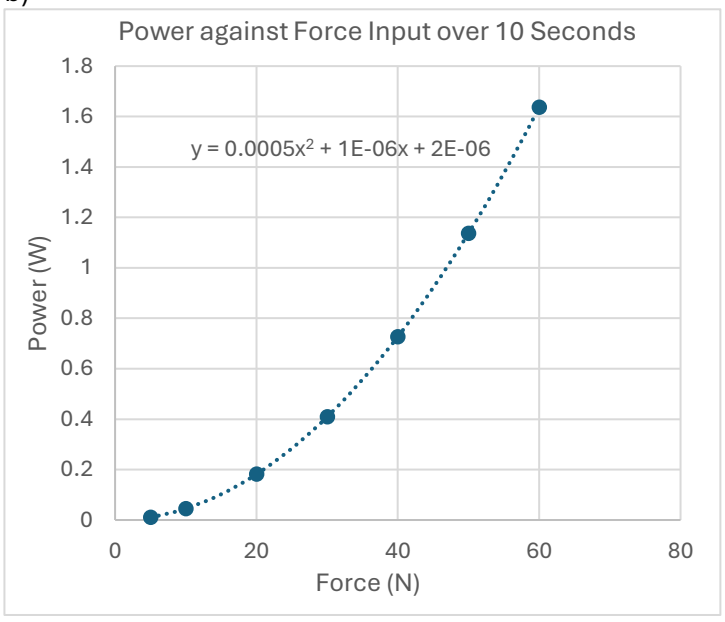

Figure 4.1: Data collected from Simulink model a) Voltage output against force input at 2.75Hz in one oscillation b) Power output against force input at 2.75Hz over 10 seconds

$$P = \frac{{d_{33}}^2 \cdot \omega}{\tan(\delta) \cdot C_{Total}} F^2$$

Equation 4.3

Relationship between power output and force input, derived in Appendix B

Effect of Frequency on Power Output

It is crucial to evaluate how varying the frequency of applied force affects the power output of the piezoelectric energy harvesting system to find the optimum load profile for power generation. The system was simulated using a constant input force (60N) and lever ratio, with the frequency varied from 1.4 to 4.0 Hz. The results are presented in Figures 4.2a and 4.2b.

As shown in Figure 4.2a, the power output per oscillation decreases nonlinearly with increasing load frequency. At lower frequencies (1.4-2 Hz), the system generates significantly more energy per cycle reaching over 0.12W at 1.4Hz. This value falls rapidly to 0.041W at 4Hz. This observed trend is due to the shortened time available for the piezoelectric elements to respond at higher frequencies. As frequency increases, the applied force ramps and unloads more rapidly, resulting in narrower voltage peaks and less total per output per oscillation.

Despite the sharp decline in the single oscillation output, Figure 4.2b shows that total energy harvested over 10 seconds remains approximately constant, with values consistently hovering at 1.6W across all frequencies. This occurs as although each cycle produces less energy at higher frequencies, more cycles occur per second. Thus, the reduced energy per oscillation is offset by the increased frequency of loading, resulting in a flat total power output curve.

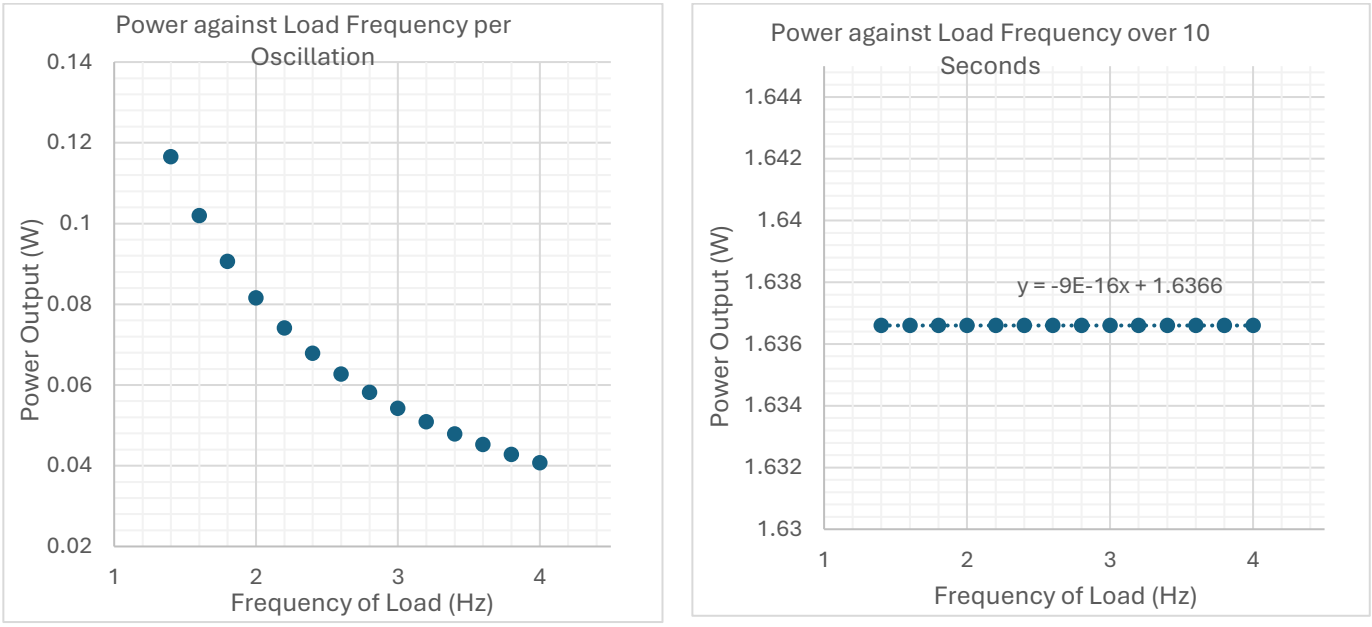

Figure 4.2: Exploring power relationships using data from the Simulink model a) Voltage output against force input at 2.75Hz in one oscillation b) Power output against force input at 2.75Hz over 10 seconds

Limitations of the Model

While the Simulink model provides valuable insight into the theoretical performance of the piezoelectric regenerative system, it is important to acknowledge several limitations that affect the real-world validity of the results.

Firstly, this model operates under loss-free conditions, assuming perfect transduction form mechanical to electrical energy. Real-world systems, on the other hand, are subject to mechanical losses, electrical losses and material imperfections. These can come in the form of friction, damping, resistance and dielectric leakage which are inherent in electromechanical systems. By neglecting these factors, the model overestimates the system's power output, especially at higher input forces or sustained frequencies where losses would compound.

Another limitation is the simulation used material property values which are accurate at the resonant frequency. While this maximises theoretical output, real world excitation is often irregular and the system operates at many frequencies, meaning sustained resonance is unlikely. Therefore, performance in practice may fall short of simulation expectations.

Furthermore, the input forces applied in the model follow a clean, symmetrical sinusoidal waveform. In reality, vehicle suspension inputs are asymmetrical, impulsive or random, particularly over rough terrain. These unmodelled dynamics could significantly alter the timing and consistency of voltage peaks, affecting both the per-cycle and total energy transduction.

Finally, the simulation models the piezoelectric elements as having constant d_{33} and capacitance values. However, real materials exhibit environmentally dependant properties, especially under prolonged cyclic loading and the variety of conditions it will operate within.

Despite these limitations, the Simulink model has successfully identified key trends in system behaviour, particularly the relationships between force, frequency of loading and outputted power. However, to validate these insights and determine real-world viability, physical testing of a prototype will be key. This will allow for comparison between simulated and experimental results, helping to quantify losses, confirm theoretical predictions and inform future design improvements.

4.2 Practical Testing

A core aim of the project was to investigate the real-world relationship between applied force, speed and electrical response of a piezoelectric transducer (PZT) under dynamic loading conditions. After practical data collection, analysis was undertaken focusing on voltage-time integrals, peak voltage behaviour and power/energy output calculations. Understanding these

relationships is crucial for optimising PZT-based energy harvesting and the applicability of the system. Selected tests were use for analysis, however, the entirety of results can be found in Annex C.

Voltage-Time Integral Analysis

The voltage-time integral represents the total electrical response of the system, both the maximum applied force and application speed's effect were analysed. The results provide insight into the relationship between mechanical input and electric energy generation.

Effect of Force on Voltage Output

The relationship between total voltage output and applied force at a constant speed of 100mm/minute is shown in Fig 4.3a. The results demonstrate a strong linear correlation, with the voltage-time integral increasing proportionally to applied force. The trend is represented by the linear equation in equation 4.4, where V is voltage and F is the applied force.

$$V = 0.0384F - 0.3864$$

Equation 4.4

where V is the total voltage output (V·s) and F is the applied force (N). The linear trend suggests that mechanical stress on the PZT is directly responsible for increased electrical output, reinforcing the expected piezoelectric output shown in equation 4.5a. The gradient represents the electromechanical transduction efficiency of the piezoelectric element, and the small negative intercept (-0.3864) may result from system noise, fixture compliance or an activation threshold for measurable voltage output.

By equating the linear relationship of force and voltage output to equation 4.5a, the gradient represents the experimentally measured value of $\frac{d_{33}}{C_{Total}}$ and d_{33} is calculated using equation 4.5b. The total capacitance of the system is known, calculated as four times the capacitance of a single PZT element due to the parallel configuration. Since the technical datasheet for this PZT composition (shown in Appendix D) does not specify a d_{33} value, standard values for PZT-4 and PZT-8 are used for comparison. This allows for evaluation of the efficiency of electromechanical transduction in the system. The experimental value 138.2 pC/N, calculated in equation 4.2b, is significantly lower than standard values for PZT-4 (285 pC/N) and PZT-8 (225 pC/N) (Table 3), indicating a system inefficiency between 48.5% and 61.4%.

However, this does not solely indicate inherent energy loss but rather reflects possible differences in material composition, mechanical constraints and the method of measurement. PZT-4 and PZT-8 are trademarked compositions, meaning the PZT elements used in this study do not have

an identical formulation to these materials. However, since many hard PZT compositions share similar electromechanical characteristics, PZT-4 and PZT-8 serve as reasonable reference materials for estimating expected performance. The lower experimentally determined d_{33} value suggests that PZT elements in this study have been curated for enhanced mechanical durability at the expense of charge generation efficiency. Additionally, mechanical limitations, such as fixture compliance and restricted deformation, could have limited the full charge generation of the piezoelectrics. This may have originated from slight deformation under load of PLA components and solder on the PZT elements effecting the load distribution for example.

Thus, while the system efficiency appears lower than expected, this is likely partly due to material composition differences and experimental constraints rather than solely energy losses. Future work should include direct d_{33} measurements of the PZT to refine the performance evaluation

a)

$$V_{Total} = \frac{d_{33}}{C_{Total}} F$$

b)

$$\frac{d_{33}}{C_{Total}} = 0.0384$$

$$d_{33} = 0.0384 \cdot 4C_{Single}$$

$$d_{33} = 138.2\ pC/N$$

Equation 4.5: a) Relationship between voltage output and force input, derived in Appendix B b) Experimentally calculated d_{33} value

Effect of Speed on Voltage Output

The equation relating movement speed (S) and total voltage output (V) (equation 4.6), with an applied force of 50N, is shown in Figure 4.3b.

$$V = -0.0015S + 1.6782$$

Equation 4.6

The data demonstrates a nearly constant voltage output across all tested speeds, with the gradient representing negligible variations across different tests. This suggests that strain rate does not significantly influence the electrical response, meaning that force application, rather than the rate of force change, is the primary determinant of energy generations.

While the voltage-time integral provides insight into total charge displacement, it is also important to examine instantaneous voltage behaviour to assess the system's response to force application. This is further analysed through peak voltage measurements.

Peak Voltage Analysis

Peak voltage is a key parameter in assessing the instantaneous electrical response of the piezoelectric system under applied load. A linear relationship between force and voltage is expected due to the direct relationship between stress and induced charge generation.

a)

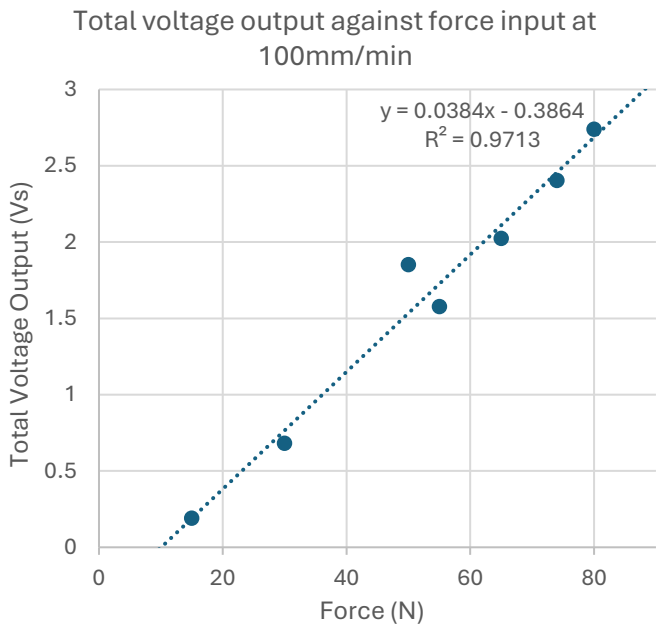

b)

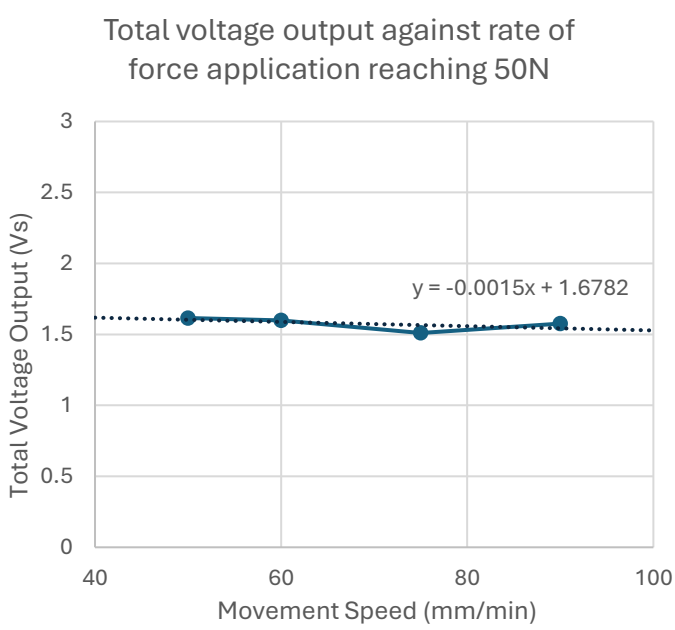

Figure 4.3 a) Voltage output against force input at 100mm/min b) Voltage output against rate of force application reaching 50N

Figure 4.2c illustrates that peak voltage increases linearly with force up to 60N, consistent with expected piezoelectric behaviour. Beyond this, voltage saturates at approximately 0.2V, despite increasing force. This plateau aligns with the 15N per-element force rating (shown in Appendix X), as the elements are arranged in parallel their operational limit is 60N. Therefore, after 60N, additional force does not translate into higher charge generation, likely due to the saturation of dipole alignment within the PZT domains. Hard PZT materials such as this exhibit limited domain reorientation beyond a certain stress threshold, preventing further charge displacement. The plateau behaviour reflects a limitation not accounted for in the Simulink model, where the force-voltage relationship is assumed linear indefinitely. In practice, material limits and domain saturation introduce nonlinearities, confirming the importance of experimental validation.

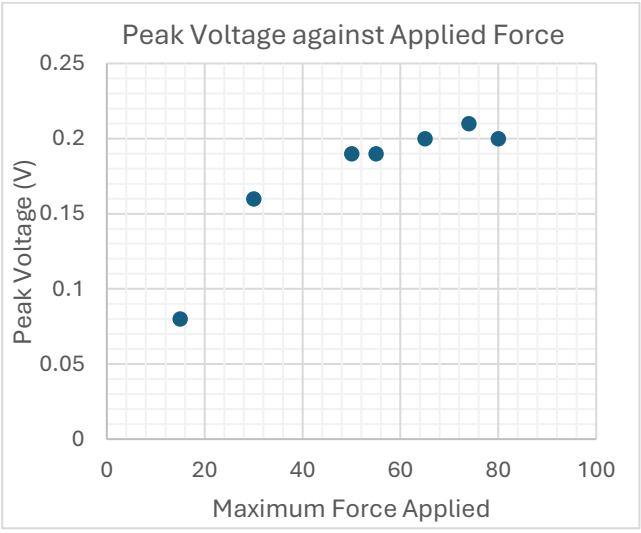

Figure 4.4 Peak positive voltage across all tests, observed at 100mm/min movement speed

Power

Power output is the most critical metric in assessing the regenerative system, as it represents the total usable energy supplied to the vehicle. While voltage provides insight into piezoelectric behaviour, the power determines real-world applicability. Understanding how force influences power generation is key to optimising energy recovery and improving system efficiency for practical implementation.

The theoretical relationship suggests that power should scale quadratically with force following equation 4.9b, where V is the voltage output per oscillation and R is the total resistance of the system. Given that voltage is linearly related to force ($V \propto F$), power is expected to have a quadratic relationship with force ($P \propto F^2$).

Figure 4.5a confirms this expected behaviour, and equation 4.7 shows that energy output per oscillation increases quadratically with input force following the trend:

$$E = 3 \times 10^{-5}F^2 + 0.0011F - 0.0235 \quad (R^2 = 0.9987)$$

Equation 4.7

Where E is the energy generated per oscillation (in Joules) and F is the peak applied force (N). The coefficient of determination ($R^2 = 0.9987$) against a second-order polynomial trendline indicates a strong quadratic correlation, mirroring the theoretical relationship shown in the Simulink model. However, this equation includes a negative linear component (0.0011F) which was absent in the simulation and suggests minor energy dissipation effects, likely from dielectric loss or charge leakage. The small intercept (-0.0235) points to a baseline energy output even at low forces, possibly due to background mechanical vibrations or electrical noise present on the oscilloscope.

However, Figure 4.5b, which plots power per oscillation against input force, reveals a linear relationship (equation 4.8).

$$P = 0.0001F - 0.0014 \quad (R^2 = 0.9906)$$

Equation 4.8

This diverges from the quadratic power-force relationship observed in the simulation. The cause of this deviation lies in the experimental test equipment. Although the system moved at a constant rate (100mm/min), increasing the peak force required longer displacement distances, which in turn lengthened the time taken for each oscillation. Since power is defined as energy divided by time, and the oscillation time increased with force, this resulted in a linear power trend. Importantly, this proves that if the oscillation frequency has remained consistent, the energy increase observed would have translated into a quadratic power relationship, as seen in the

Simulink model. The linearity of the power curve therefore reflects an effect of testing conditions rather than a flaw in the underlying transduction functionality.

The negative intercept in the power trend (-0.0014W) suggests a threshold effect, and the high R^2 value confirms the confirmation to the fitted equation. This result highlights the importance of capturing time-dependent effects in real-world systems and confirms that under consistent-frequency conditions, the physical system would behave in close alignment with theoretical and simulated expectations.

a)

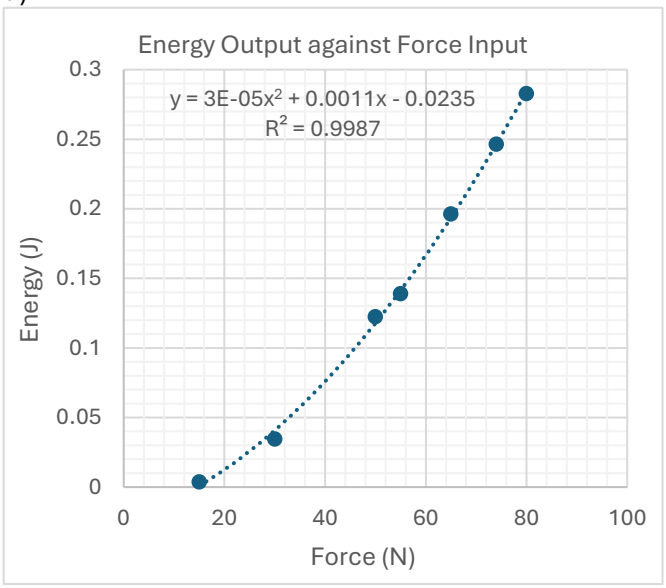

b)

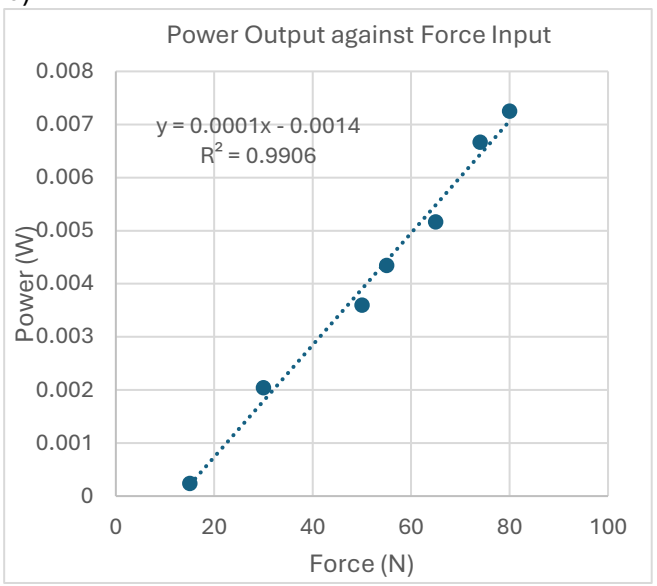

Figure 4.5 a) Graph showing the relationship between energy output per oscillation and force input at 100mm/min b) Graph showing the relationship between power output per oscillation and force input at 100mm/min

The resistance of the PZT system was calculated using Equation 4.9a. In this equation, tan(δ) represents the dielectric loss, C_{Total} is the total capacitance (four times the capacitance per element due to the parallel configuration) and ω is the angular frequency, determined using the resonant frequency. These parameters, specified in the PZT datasheet (Appendix D), directly influence the systems electrical characteristics and efficiency.

Despite the observed consistent quadratic increase in energy output, several efficiency losses limit the system's performance at high loads. Dielectric loss is the ratio of resistance to reactance and is a measure of heat generation under dynamic loading [20]. Therefore, it accounts for energy dissipation as heat within the PZT element, reducing the proportion of mechanical energy converted into electrical output, and inherently lowering efficiency. The energy loss is furthered by heat generation scaling quadratically with force and proportionally to power, leading to exponential increases at higher forces. This could negatively impact performance by raising material temperature, leading to temperature-induced drift in piezoelectric performance,

affecting long-term system stability and energy conversion efficiency. While mechanical compliance has already been discussed, its impact on power output remains relevant, as non-uniform force application may reduce energy conversion efficiency.

The results confirm that power output scales quadratically with applied force, aligning with theoretical expectations and reinforcing the viability of piezoelectric energy harvesting in dynamic systems. However, despite this consistent increase, efficiency limitations are expected to become more significant at higher forces, particularly due to dielectric losses and heat generation. These complications introduce a scaling challenge, as excessive thermal buildup could alter piezoelectric response and long-term material stability, ultimately affecting energy conversion efficiency. Therefore, practical implementation will require further consideration of how the design choices work to mitigate these issues in real-world applications.

a)

$$R = \frac{\tan(\delta)}{\omega C_{Total}}$$

$$R = \frac{0.004}{201{,}062 \cdot 4(0.9 \times 10^{-6})} = 5.53\Omega$$

b)

$$P = \frac{V^2}{R}$$

Equation 4.9: a) Calculating the electrical resistance of the PZT elements [40] b) Calculating the total power output

In automotive applications, where suspension forces fluctuate dynamically, understanding how these variations influence total energy recovery is essential. The following section will explore the scalability of the system, assessing its feasibility when integrated into a vehicle and evaluating its contribution to overall energy efficiency.

5. Applicability to Automotive Implementation

5.1 Introduction

It is crucial to assesses the real-world applicability of the system developed through both simulation and practical testing. It critically examines the potential contribution of the system's power output relative to typical automotive energy demands, evaluates cost and integration challenges and reflects on the physical model's performance under realistic conditions. Finally, it considers the broader viability of this technology by weighing its technical strengths and limitations, economic feasibility and environmental implications within the context of future vehicle platforms.

5.2 Power Output and Potential Energy Savings

Estimating Scaled Power Output

In full-size passenger vehicles, the suspension system frequently encounters force magnitudes between 400 and 900 N per corner, rising hugely under extreme driving conditions. Given the prototype's confirmed quadratic behaviour with force input, power output is expected to increase significantly with these elevated loads. For example, using equation 4.7, relating energy and force, a force of 700N would yield approximately 15.4J. Assuming a typical oscillation frequency of 2.75Hz per wheel (midpoint of sprung mass frequency range 1.5 – 4 Hz [32), and a four-wheel vehicle design, the total energy harvested per second would be 169.4W. This calculated value is assuming that various other properties of the system would stay consistent with the prototype, dielectric coefficient and efficiency in transfer of power for instance. However, when scaling up to a full-size model, utilising higher load and more efficient PZT elements, aluminium for the frame instead of PLA and more rigid joining techniques would further improve the efficiency of the system. This results in the realistic value when full-sized to be higher than the calculated 169.4W.

To evaluate the practical relevance of the power generated by this piezoelectric system, it is important to compare it against the energy demand of a real vehicle. An analysis of energy consumption in a plug-in hybrid electric vehicle (PHEV), tested over 5000km of real-world driving conditions found the average energy consumption in electric mode was 208Wh/km [41]. If the system harvested 169.4W continuously during motion, at 50km/h urban driving this yields 3.39Wh/km. This value is approximately 1.6% of the total energy consumption of the PHEV in electric mode. While this appears low, the energy is passively harvested from motion that already occurs during driving, that would otherwise be wastefully dissipated.

Rather than charging the battery solely, the system could be used to support low-power subsystems such as lighting, cabin electronic, monitoring systems or auxiliary battery trickle charging. In doing so, the system can offset parasitic loads on the primary battery, contributing to small but measurable efficiency gains. Over time, and particularly in fleet vehicles or public transport systems, small energy savings can compound into substantial fuel efficiency improvements [4].

Therefore, while the system may not significantly extend driving range on its own without further development, its potential as a continuous and non-intrusive energy source justifies further exploration.

5.3 Cost-Efficiency and Practical Integration

Beyond theoretical performance and power output, the real-world adoption of a regenerative suspension system depends heavily on its cost-effectiveness, manufacturability and ease of integration into existing vehicle platforms.

Material and Component Costs

One of the primary cost drivers of the prototype is the use of piezoelectric elements, specifically TDK PowerHap actuators. While these elements offer high mechanical strength, fast response and large displacement, they are relatively expensive compared to traditional structural materials. In the prototype, only four PZT elements were used per corner, however, a full-scale system may require a larger array, multi-layer configurations or more advanced piezoelectric materials to handle increased force and displacement demands while avoiding saturation.

Furthermore, the current prototype uses PLA plastic for its structural components due to cost and simplicity of 3D printing. While sufficient for experimental validation, PLA lacks the mechanical strength and durability required for automotive conditions. As previously mentioned, a real world system would require structural components to made from aluminium, increasing both material and manufacturing costs.

5.4 Manufacturing and Assembly

From a manufacturing perspective, the system is composed of relatively simple components: levers, elastic dampeners, fasteners and a force transmitting clock. These can be easily adapted for mass production using conventional casting, stamping or CNC processes. The modular nature of the design, particularly the isolation of the piezoelectric unit from the main suspension structure, would allow for drop-in integration into existing damper locations, minimising the need for suspension system redesigns. The system's compact size and absence of active electronics (in its base configuration) also reduce the complexity of installation. Integration into subframes or damper mounts is feasible with minimal alteration in the assembly line. In electric vehicles, where space and weight are often tightly optimised, the systems low weight and passive operation provide a significant advantage over bulkier electromagnetic alternatives.

5.5 Integration into Electrical Architecture

The harvested energy can be stored in small supercapacitor banks or auxiliary batteries and routed through basic rectification and regulation circuits. The electrical architecture required is comparable in complexity to that of sensor or lighting circuits. Crucially, because the piezoelectric system does not rely on precise external control, its integration into the vehicle's electrical system can remain largely isolated, avoiding the need for communication with the ECU.

5.6 Cost-Benefit Assessment

While the initial implementation cost may be relatively high, primarily due to piezoelectric elements, the long operational life, lack of moving parts and passive recovery make the system attractive for long-term use. The cost per watt recovered may be higher than alternative energy recovery systems, such as regenerative braking, however the continuous, always harvesting nature enables consistent returns during any scenario. This system will be best suited to two groups in particular. Firstly, fleet vehicles, buses or taxis with predictable usage patterns and high annual mileage, maximising the harvesting of the system. Secondly, high-end hybrid or electric vehicles, where marginal range extensions contribute to competitive advantage.

5.7 Conclusion

The investigation conducted through both simulation and physical testing has demonstrated that piezoelectric regenerative suspension systems present a viable means of capturing vibrational energy within passenger vehicles. While the power output in its current prototype form is modest, extrapolated full-scale estimations show promising potential, particularly under high loading scenarios where suspension loads reach upwards of 700N per corner. Under these conditions, total power outputs could exceed 150W, sufficient to contribute meaningfully to offsetting auxiliary vehicle loads.

6. Recommendations for Further Work

The development of the proposed regenerative suspension system has demonstrated strong potential for real-world automotive applications. However, further research and testing are necessary to enhance its durability, efficiency and feasibility at full scale. The following key areas are recommended for future research to optimise the regenerative suspension model and enable practical implementation.

Full scale

The first critical step to real-world deployment is scaling up the system from a prototype to a full-size functional model, however there are many complexities with scaling that will need to be considered. For example, non-linearity when scaling mechanical behaviour introduces further challenges that require large changes within the system. The load increases with the cube of the scaling factor (27x increase) and therefore, for a reliable full-scale system a transition to aluminium alloys drastically improves the strength-to-weight ratio. This increase in strength is furthered through the improved joining techniques possible with aluminium, distributing loads more effectively. The stiffness of elastic materials scales differently from the force, typically with

the square of the scaling factor. As a result, standard elastic elements may not be sufficient in a full-scale model. Therefore, it may require utilising custom high-load elastic variants in a full-scale model. These complexities present challenges, however with sufficient planning they are possible to overcome using materials and methods commonly found in automotive manufacturing.

Integration into a vehicle suspension area,

To integrate the full-scale model into a vehicle to gather real world data of how the system performs requires further development of the model. Firstly, to remain modular and applicable across multiple vehicle models, the design must be adaptable to fit common geometries of vehicle mounting points. This would allow for a cost-effective manufacturing process as one design would be effective across the highest number of units possible effectively leveraging economies of scale for mass production. Given its placement within the wheel well, the system is exposed to debris, moisture, and temperature fluctuations. To ensure long-term reliability, protective measures should be implemented. One method is through sealed protective casing, similar to those used in shock absorbers and high-voltage battery enclosures, preventing mechanical wear and environmental damage. This protection can be furthered through impact-resistance housing, taking inspiration from undertray panels which will withstand high load impacts that would otherwise damage components.

7. Conclusion

This project has demonstrated that vibrational energy in suspension systems represents a viable but underutilised source of energy recovery in vehicles. By integrating piezoelectric elements into a compact, modular suspension assembly, it is possible to passively convert kinetic energy from road-induced oscillations into usable electrical power. Both Simulink simulations and physical testing confirmed that output energy scales predictably with applied force, following a strong quadratic relationship in controlled conditions.

Although the experimental prototype yielded modest power outputs, full-scale extrapolation, factoring in real-world vehicle mass and force profiles, indicates potential recovery rates of over 150 W per vehicle. While this represents a small fraction of total energy consumption, it is nonetheless significant in supporting auxiliary loads, extending battery life, and reducing parasitic losses.

Challenges remain in refining material efficiency, scaling design components, and integrating the system seamlessly into production vehicles. However, the modular architecture, passive operation, and compatibility with existing vehicle subframes make piezoelectric regenerative

suspension systems a compelling candidate for future implementation. With further development and optimisation, such systems could become a valuable contributor to sustainable transport, complementing existing regenerative technologies and advancing the energy efficiency of next-generation automotive platforms.

References

[1] Dishant , P. Singh, and M. Sharma , “Suspension Systems: A Review,” *Academia.edu*, 2024. https://www.academia.edu/33456500/Suspension_Systems_A_Review

[2] Elibrary.ru, “SIMULATION AND TESTING OF ENERGY DISSIPATION IN PASSENGER VEHICLE DAMPERS,” *Elibrary.ru*, 2012. https://elibrary.ru/item.asp?id=9408881

[3] M. A. A. Abdelkareem *et al.*, “Vibration energy harvesting in automotive suspension system: A detailed review,” *Applied Energy*, vol. 229, pp. 672–699, Nov. 2018, doi: https://doi.org/10.1016/j.apenergy.2018.08.030.

[4] D. L. Chandler, “More power from bumps in the road,” *MIT News | Massachusetts Institute of Technology*, Feb. 09, 2009. https://news.mit.edu/2009/shock-absorbers-0209

[5] N. Tulsian and S. Dewangan, “A discussion on energy harvesting through suspension system,” *Materials Today: Proceedings*, vol. 79, pp. 189–192, Jan. 2023, doi: https://doi.org/10.1016/j.matpr.2022.10.052.

[6] P. Mitcheson, T. Sterken, C. He, M. E. Kiziroglou, E. M. Yeatman, and R. Puers, “Electrostatic Microgenerators,” *Measurement and Control*, vol. 41, no. 4, pp. 114–119, May 2008, doi: https://doi.org/10.1177/002029400804100404.

[7] R. T. Aljadiri, “The Principles and Applications of Electrostatic Transducers,” *Advances in civil and industrial engineering book series*, pp. 241–274, Jun. 2024, doi: https://doi.org/10.4018/978-1-6684-9214-7.ch008.

[8] I. I. Inculet, “Electrostatics in industry,” *Journal of Electrostatics*, vol. 4, no. 2, pp. 175–192, Jan. 1978, doi: https://doi.org/10.1016/0304-3886(78)90071-2.

[9] M. J. Anderson, J. A. Hill, C. M. Fortunko, N. S. Dogan, and R. D. Moore, “Broadband electrostatic transducers: Modeling and experiments,” *The Journal of the Acoustical Society of America*, vol. 97, no. 1, pp. 262–272, Jan. 1995, doi: https://doi.org/10.1121/1.412310.

[10] B. Yang *et al.*, “Electromagnetic energy harvesting from vibrations of multiple frequencies,” vol. 19, no. 3, pp. 035001–035001, Mar. 2009, doi: https://doi.org/10.1088/0960-1317/19/3/035001.

[11] A. R. M. Siddique, S. Mahmud, and B. V. Heyst, “A comprehensive review on vibration based micro power generators using electromagnetic and piezoelectric transducer mechanisms,” *Energy Conversion and Management*, vol. 106, pp. 728–747, Dec. 2015, doi: https://doi.org/10.1016/j.enconman.2015.09.071.

[12] J. F. Tressler, S. Alkoy, and R. E. Newnham, “Piezoelectric Sensors and Sensor Materials,” *Journal of Electroceramics*, vol. 2, no. 4, pp. 257–272, 1998, doi: https://doi.org/10.1023/a:1009926623551.

[13] S. Chen *et al.*, “Piezocatalytic Medicine: An Emerging Frontier using Piezoelectric Materials for Biomedical Applications,” *Advanced materials*, vol. 35, no. 25, Apr. 2023, doi: https://doi.org/10.1002/adma.202208256.

[14] M. C. Sekhar, E. Veena, N. S. Kumar, K. C. B. Naidu, A. Mallikarjuna, and D. B. Basha, “A Review on Piezoelectric Materials and Their Applications,” *Crystal Research and Technology*, p. 2200130, Nov. 2022, doi: https://doi.org/10.1002/crat.202200130.

[15] X. D. Xie and Q. Wang, “Energy harvesting from a vehicle suspension system,” *Energy*, vol. 86, pp. 385–392, Jun. 2015, doi: https://doi.org/10.1016/j.energy.2015.04.009.

[16] B. Bera and M. Das Sarkar, “Piezoelectric Effect, Piezotronics and Piezophototronics: A Review,” *Imperial Journal of Interdisciplinary Research (IJIR)*, vol. 2, no. 11, pp. 2454–1362, 2016, Available: https://www.static-contents.youth4work.com/y4w/6551d788-6266-4e1c-9948-40a29d8792da.pdf

[17] A. Arnau and D. Soares, “Fundamentals of Piezoelectricity,” *Piezoelectric Transducers and Applications*, pp. 1–38, doi: https://doi.org/10.1007/978-3-540-77508-9_1.

[18] Y. Saigusa, “Quartz-Based Piezoelectric Materials,” *Advanced Piezoelectric Materials*, pp. 197–233, 2017, doi: https://doi.org/10.1016/b978-0-08-102135-4.00005-9.

[19] K. Uchino, “The Development of Piezoelectric Materials and the New Perspective,” *Advanced Piezoelectric Materials*, pp. 1–92, 2017, doi: https://doi.org/10.1016/b978-0-08-102135-4.00001-1.

[20] T. Jordan, “Piezoelectric Ceramics Characterization,” Sep. 2001. Available: https://www.cs.odu.edu/~mln/ltrs-pdfs/icase-2001-28.pdf

[21] H. JAFFE, “Piezoelectric Ceramics,” *Journal of the American Ceramic Society*, vol. 41, no. 11, pp. 494–498, Nov. 1958, doi: https://doi.org/10.1111/j.1151-2916.1958.tb12903.x.

[22] K. Uchino, *Advanced Piezoelectric Materials*, 2nd ed. Elsevier Science, 2017. Available: https://www.google.co.uk/books/edition/Advanced_Piezoelectric_Materials/QJipDQAAQBAJ?hl=en&gbpv=1&dq=piezoelectric+materials&pg=PP1&printsec=frontcover

[23] K. KAKEGAWA, J. MOHRI, S. SHIRASAKI, and K. TAKAHASHI, “Sluggish Pansition Between Tetragonal and Rhombohedral Phases of $Pb(Zr,Ti)0_3$ Prepared by Application of Electric Field,” *Journal of the American Ceramic Society*, vol. 65, no. 10, pp. 515–519, Oct. 1982, doi: https://doi.org/10.1111/j.1151-2916.1982.tb10344.x.

[24] B. W. Lee and E. J. Lee, “Effects of complex doping on microstructural and electrical properties of PZT ceramics,” *Journal of Electroceramics*, vol. 17, no. 2–4, pp. 597–602, Dec. 2006, doi: https://doi.org/10.1007/s10832-006-8568-2.

[25] Y. Saito *et al.*, “Lead-free piezoceramics,” *Nature*, vol. 432, no. 7013, pp. 84–87, Oct. 2004, doi: https://doi.org/10.1038/nature03028.

[26] T. Ibn-Mohammed *et al.*, “Life cycle assessment and environmental profile evaluation of lead-free piezoelectrics in comparison with lead zirconate titanate,” *Journal of the European Ceramic Society*, vol. 38, no. 15, pp. 4922–4938, Dec. 2018, doi: https://doi.org/10.1016/j.jeurceramsoc.2018.06.044.

[27] T. Ibn-Mohammed, S. C. L. Koh, and I. M. Reaney, “Integrated hybrid life cycle assessment and supply chain environmental profile evaluations of lead-based (lead zirconate titanate) versus lead-free (potassium sodium niobate) piezoelectric ceramics,” *Energy & Environmental Science*, Aug. 21AD, doi: https://doi.org/10.1039/C6EE02429G.

[28] S. S. Anandakrishnan *et al.*, “Recycling hazardous and energy-demanding piezoelectric ceramics using an oxide–halide perovskite upside-down composite method,” *RSC Sustainability*, vol. 2, no. 4, pp. 961–974, Apr. 2024, doi: https://doi.org/10.1039/D3SU00348E.

[29] European Union, “EUR-Lex - 32000L0053 - EN - EUR-Lex,” *Europa.eu*, 2020. https://eur-lex.europa.eu/legal-content/EN/TXT/?uri=celex%3A32000L0053

[30] T. Ibn-Mohammed *et al.*, “Life cycle assessment and environmental profile evaluation of lead-free piezoelectrics in comparison with lead zirconate titanate,” *Journal of the European Ceramic Society*, vol. 38, no. 15, pp. 4922–4938, Dec. 2018, doi: https://doi.org/10.1016/j.jeurceramsoc.2018.06.044.

[31] X. D. Xie, N. Wu, K. V. Yuen, and Q. Wang, “Energy harvesting from high-rise buildings by a piezoelectric coupled cantilever with a proof mass,” *International Journal of Engineering Science*, vol. 72, pp. 98–106, Nov. 2013, doi: https://doi.org/10.1016/j.ijengsci.2013.07.004.

[32] M. Agostinacchio, D. Ciampa, and S. Olita, “The vibrations induced by surface irregularities in road pavements – a Matlab® approach,” *European Transport Research Review*, vol. 6, no. 3, pp. 267–275, Dec. 2013, doi: https://doi.org/10.1007/s12544-013-0127-8.

[33] Toyota, “PRIUS TECHNICAL SPECIFICATIONS HYBRID SYNERGY DRIVE .” Available: https://media.toyota.co.uk/wp-content/uploads/sites/5/2021/03/1614162945210222MPriusTechSpec.pdf

[34] Toyota, “RAV4 TECHNICAL SPECIFICATIONS,” *Toyota.co.uk*. https://media.toyota.co.uk/wp-content/uploads/sites/5/pdf/220203M-RAV4-Tech-Spec.pdf

[35] Honda, “Honda CR-V specifications, dimensions and grades,” *www.honda.co.uk*. https://www.honda.co.uk/cars/new/cr-v-hybrid-suv/specifications.html

[36] TDK, “Piezo Haptic Actuators -PowerHap Actuators with Adjustable Haptic Feedback,” TDK, 2023. Available: https://product.tdk.com/system/files/dam/doc/product/sw_piezo/haptic/powerhap/data_sheet/20/10/ds/1313h018v120.pdf

[37] L. H. Fang, R. bin A. Rahim, M. I. F. Romli, M. Z. Zakariya, J. B. A. M. Jobran, and N. B. Kimpol, “Piezoelectric Array Configuration Technique into Enhance Power Catchment for Sound Energy Harvester System,” *IEEE Xplore*, Nov. 01, 2020. https://ieeexplore.ieee.org/document/9306122

[38] “Tinius Olsen H1KS Benchtop Tester Rentals,” *Advanced Test Equipment Corp. - ATEC*, 2023. https://www.atecorp.com/products/tinius-olsen/h1ks?srsltid=AfmBOoqxTRasKTQd30cTwMRumPZfuh0jzjsZDLyQLZeuQRfwZagMsjUC

[39] Tektronix, “] https://www.testequipmenthq.com/datasheets/TEKTRONIX-MSO2024-Datasheet.pdf,” Available:] https://www.testequipmenthq.com/datasheets/TEKTRONIX-MSO2024-Datasheet.pdf

[40] BlackMelon, “Dissipation Factor of a Capacitor,” *All About Circuits*, Jan. 15, 2023. https://forum.allaboutcircuits.com/threads/dissipation-factor-of-a-capacitor.191427/

[41] J. Mamalaa and M. Grabaa, “Eksploatacja i Niezawodnosc – Maintenance and Reliability,” *Bibliotekanauki.pl*, vol. 23, no. 4, 2024. [Online]. Available: https://bibliotekanauki.pl/articles/2038048.pdf

Appendices

Appendix A

Table 1: Simulink Power Model Variables

Variable	Value	What is it
LR	0.5-2	Represents the lever ratio, determining the force translated from the input to the piezoelectric elements. It is varied in accordance with the force input to ensure the elements aren't overloaded.
D33	255×10^{-12} (C/N)	The dielectric constant,
C	0.9×10^{-9} F	C is the capacitance value of each PZT element
N	4	The number of piezoelectric elements

Table 2: Simulink Power Model Blocks Descriptions and Values

Parameter	Coefficient Value	Block	What it represents
Input			
Frequency	1.5-4Hz	Sine input	Road vibration range
Amplitude	120N	Sine input	Scaled weight per corner[1]
Voltage Calculation			
Lever Ratio	1/LR	Gain	Lever Ratio: The proportion of length each side of the pivot, connecting to the suspension and PZT. This effects the force and displacement delivered.
Dielectric Coefficient	D33	Gain	Dielectric Coefficient
Capacitance	1/(4*C)	Gain	Capacitance of a single PZT element. For a four-way parallel set up the total capacitance is 4C
Parallel PZT Config			
Voltage Output	Out.Voltage	ToWorkspace	Outputting the voltage data for processing in MATLAB script
1/s	$\int V$	Integrator	Integrated the voltage to find per oscillation
Squared Voltage	V^2	Product	Squaring the voltage
Resistance	1/R	Gain	Dividing the squared voltage by the resistance to calculate the power
1/s	$\int P$	Integrator	Integrated the power to find per oscillation

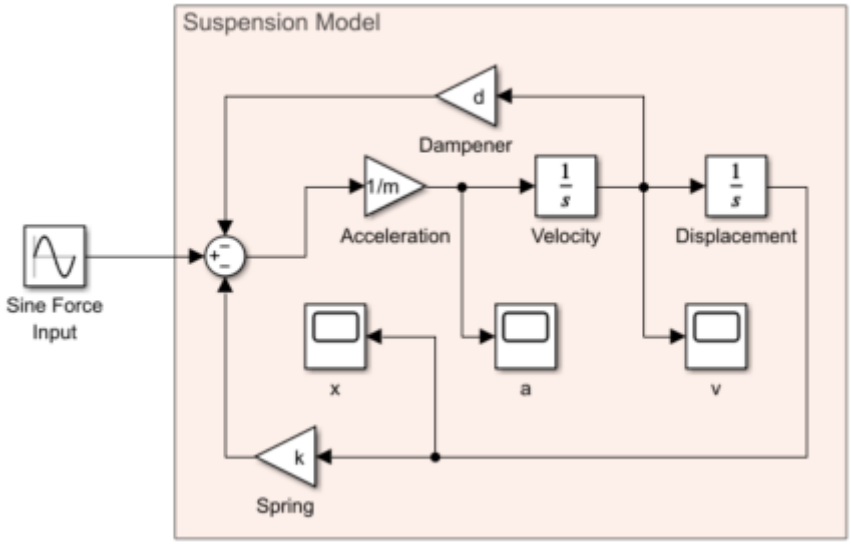

Table 3: Simulink Movement Model Block Descriptions

Parameter	Coefficient Value	Block	What it represents
Fnet	+--	Sum	Sums the totalling aspects
Acceleration	1/m	Gain	Calculates the acceleration (F/m)
Velocity	$\int a$	Integrator	Integrates the acceleration to the velocity
Dampener	d	Gain	Applies dampening force to the velocity
Displacement	$\int v$	Integrator	Integrates the velocity to the displacement
Spring	k	Gain	Applies the spring constant to the displacement

```
LR = 1;
d33 = 255*10^-12;
C = 0.9*10^-9;
N=4;
R=5.53;
m=50;
k=1985;
d=0.1;

simOut = sim('SimSuspension');

Voltage = out.Voltage;

% Extract data
time = Voltage.time;                        % Extract time values
voltage = Voltage.signals.values;           % Extract voltage signal

% Filter time range
idx = (time >= 0) & (time <= 0.25);
time_filtered = time(idx);
voltage_filtered = voltage(idx);

% Calculate instantaneous power over time
instantaneous_power = (voltage_filtered.^2) / R;

% Integrate power to get total energy (Joules)
energy = trapz(time_filtered, instantaneous_power);

% Average power over 10 seconds (W)
average_power = energy / 10;

% Display
disp(['Average Power (W): ', num2str(average_power)]);
disp(['Total Energy (J): ', num2str(energy)]);
```

Appendix B

Piezoelectric Charge Generation

$$Q = d_{33}F$$

Q = Charge Generated (C)

d_{33} *= Piezoelectric Charge Coefficient (C/N)*

F = Applied Force (N)

Voltage Output from PZT Element

$$V = \frac{Q}{C}$$

V = Voltage output (V)

Q = Charge Generated (C)

C = Capacitance of PZT Element (F)

Capacitance

$$C = \frac{\epsilon A}{t}$$

ϵ = Permittivity of Piezoelectric (F/m)

A = Electrode Surface Area (m^2)

t = Thickness of PZT Layer (m)

$$V = \frac{d_{33} F t}{\epsilon A} = \frac{d_{33} t}{\epsilon A} F = \frac{d_{33}}{C} F$$

$$P = \frac{(\frac{d_{33}}{C_{Total}} F)^2}{R}$$

$$P = \frac{(\frac{d_{33}}{C_{Total}} F)^2}{(\frac{\tan(\delta)}{\omega C_{Total}})}$$

$$P = \frac{{d_{33}}^2 \cdot \omega}{\tan(\delta) \cdot C_{Total}} F^2$$

Appendix C

Test no.	Force N	Speed mm/min	Retract mm/min	Graph	Positive V	Negative V	Total V	Dom Freq

1	50	15	250	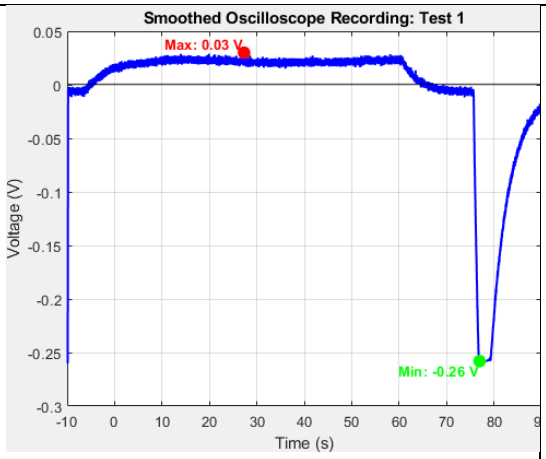	1.3010	1.8204	3.1214	0.011236
2	50	50	250	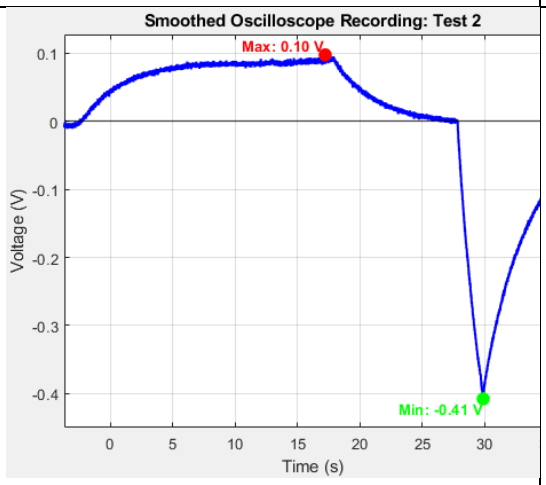	1.5042	1.6699	3.1741	0.028571
3	50	50	250	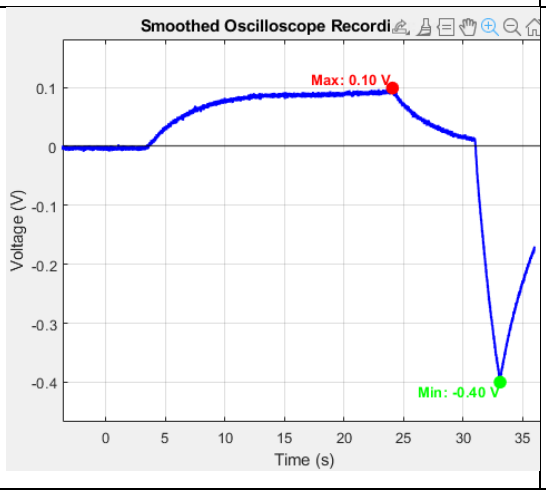	1.8175	1.2443	3.0619	0.028571

4	50	50	250	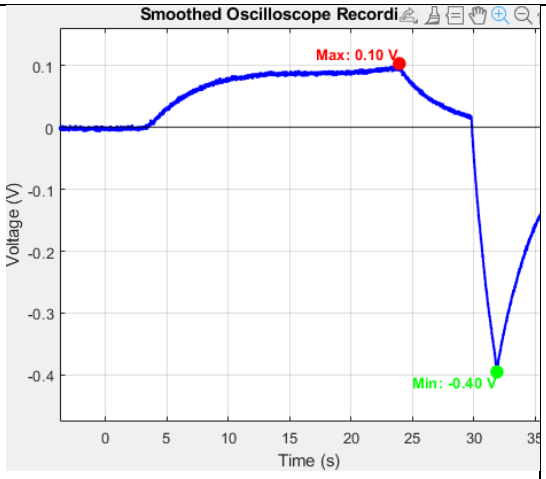	1.8141	1.3963	3.2104	0.0285 71
5	50	50	250	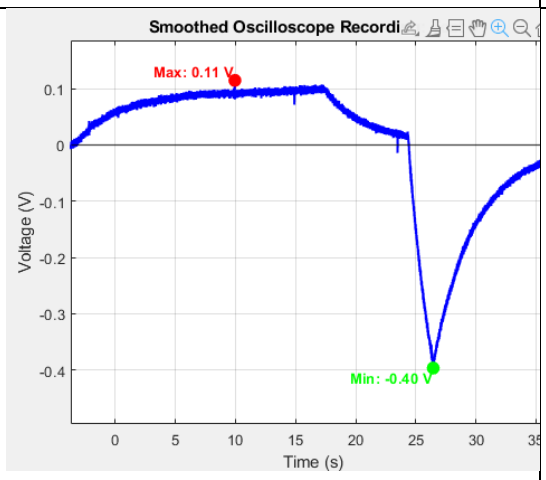	1.6154	1.7379	3.3533	0.0285 71
6	50	60	250	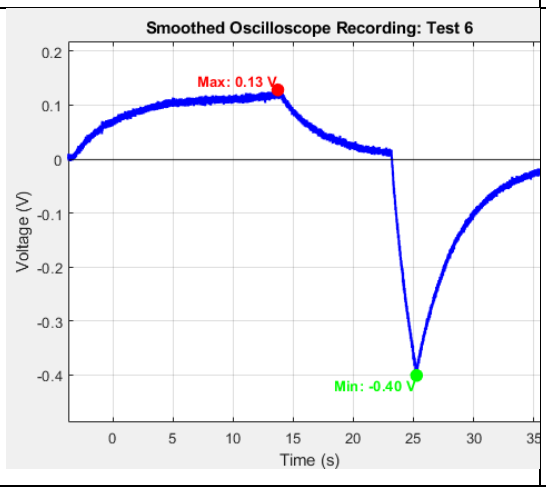	1.5994	1.7860	3.3854	0.0285 71

7	50	75	250	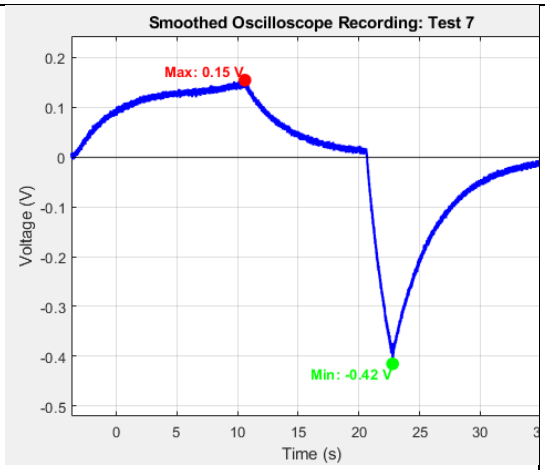	1.5097	1.8440	3.3537	0.0285 71
8	50	90	250	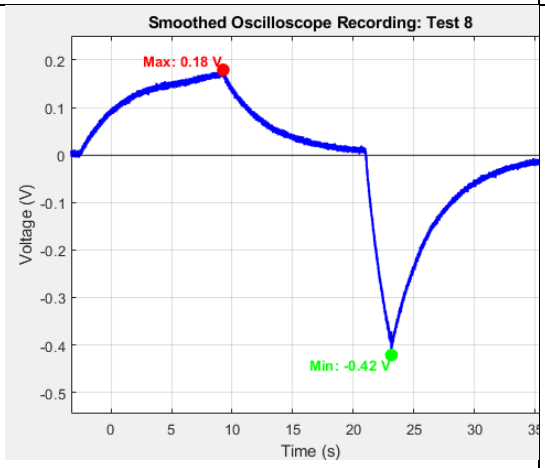	1.5749	1.8751	3.4501	0.0285 71
9	50	100	250	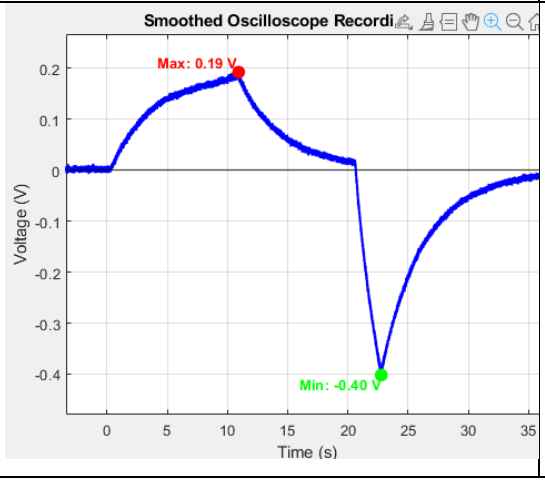	1.8526	1.8617	3.7143	0.0285 71

10	30	100	250	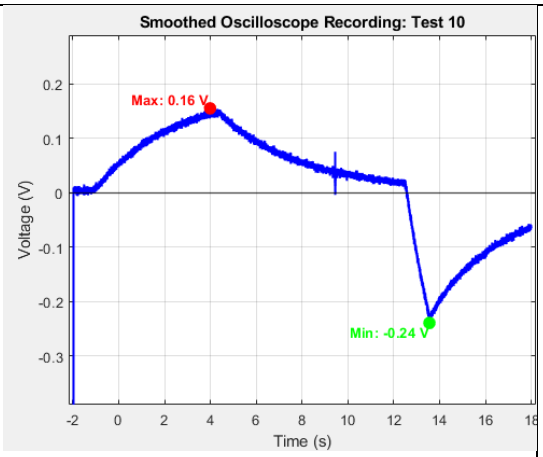	0.68102	0.68305	1.3641	0.058824
11	15	100	250	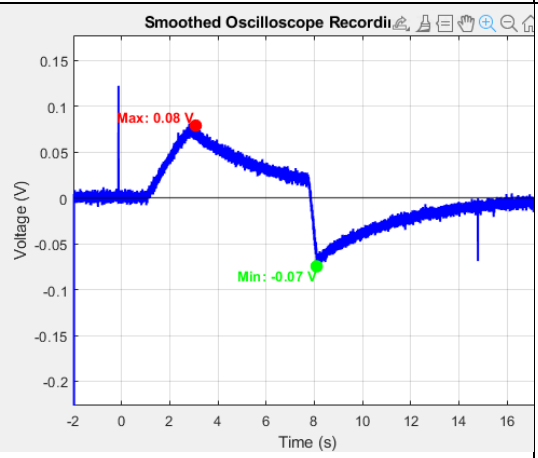	0.18962	0.22445	0.41407	0.058824
12	55	100	250	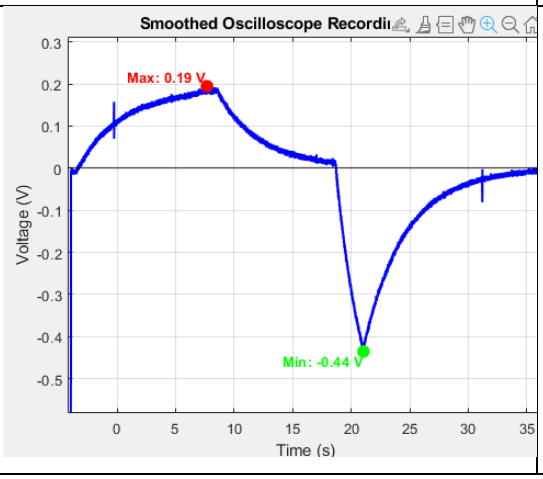	1.5777	2.0991	3.6768	0.028571

13	65	100	250	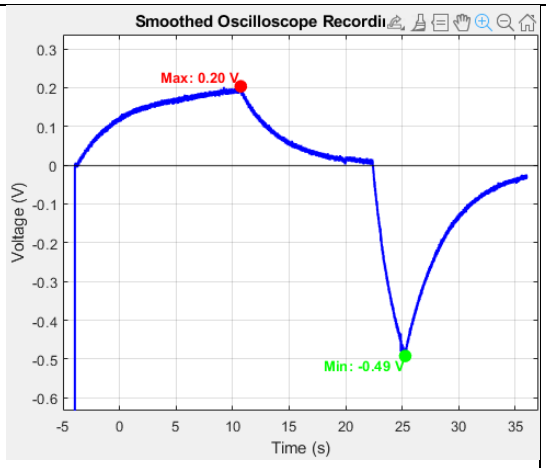	2.0244	2.5424	4.5668	0.0285 71
14	74	100	250	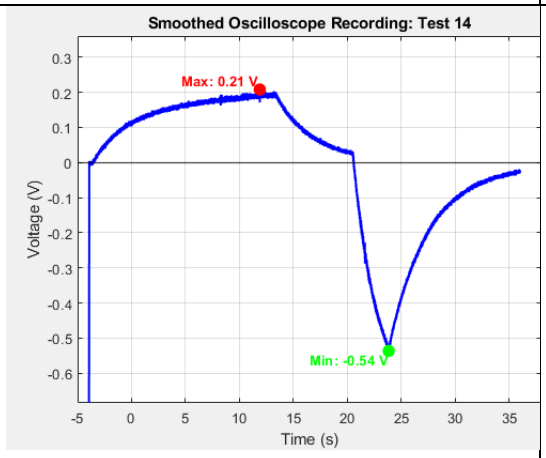	2.4025	2.9849	5.3874	0.0285 71
15	80	100	250	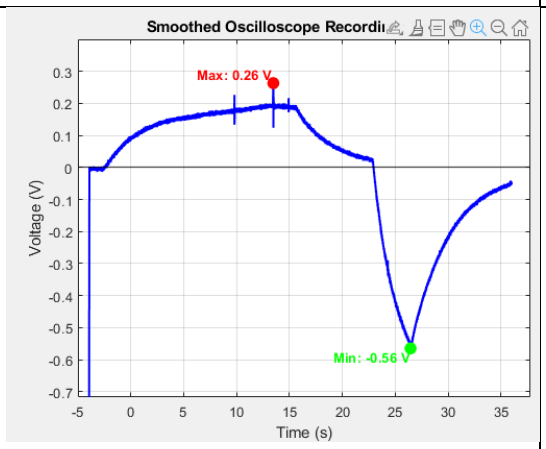	2.7398	3.1744	5.9142	0.0285 71
16	65	50	250	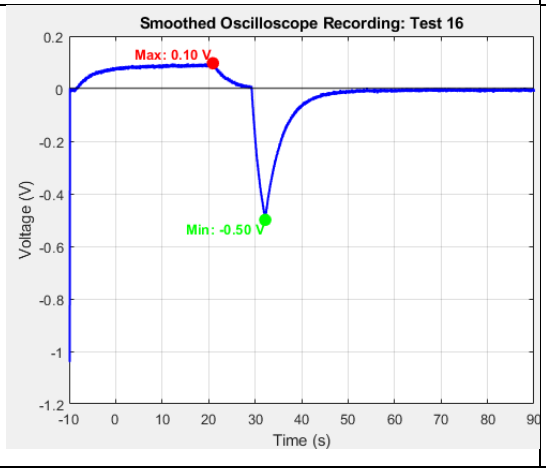	1.8089	3.0359	4.8448	0.0224 72

17	65	30	250	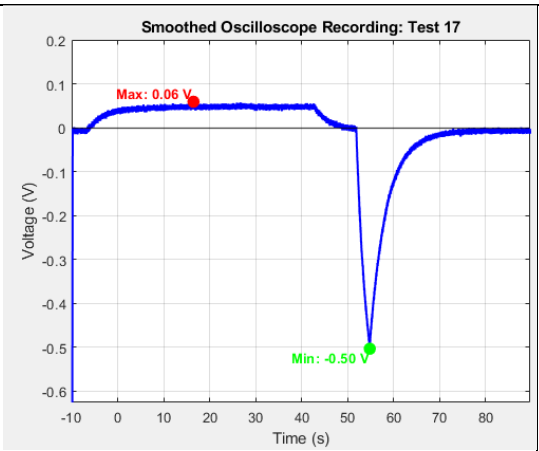	1.9832	2.9330	4.9162	0.011236

Appendix D

TDK

Piezo Haptic Actuators - PowerHap	B54102H1020A001
Actuators with Adjustable Haptic Feedback	**1313H018V120**

Features

- Large displacement
- High acceleration
- High force
- Low insertion height
- Fast response time
- Integrated sensor functionality

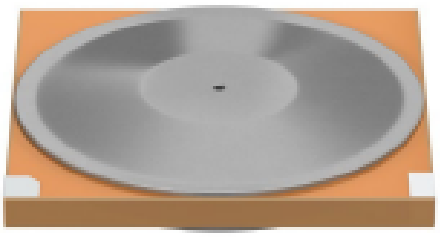

Design

- RoHS-compatible PZT (lead zirconium titanate) ceramic
- Copper inner electrodes
- Titanium cymbals for displacement amplification
- Previously known as PowerHap™ 7G
- Contains SVHC substance 12626-81-2
- Contacting: Polarized piezo element, pay attention to the positive and negative terminal.

General technical data

Parameter	Ratings
Operating voltage range	0 … 120 V
Operating temperature powered	−40 °C … +85 °C
Operating temperature unpowered	−40 °C … +125 °C
Maximum compressive force on actuator	15 N
Maximum operation frequency	The operation frequency is limited by self-heating of the device. The self-heating of device should not exceed by + 30 °C. At 120 V, 500 Hz, square wave conditions, a maximum allowable temperature increase of +30 °C is observed after about 10 s of operation.
Maximum voltage gradient	1.2 MV/s

Electrical characteristics at 25 °C

Parameter		Conditions	Expected value (typ.)
Capacitance	C	1 kHz, 1 V_{RMS}	0.9 µF
Displacement	s	0 … 120 V, measured at cymbal end-caps	65 µm
Loading charge	Q	0 …120 V	0.19 mC

TDK

Piezo Haptic Actuators - PowerHap	B54102H1020A001
Actuators with Adjustable Haptic Feedback	**1313H018V120**

Further typical electrical characteristics as a design reference for haptic applications at 25 °C[1)]

Parameter		Conditions	Typical
1st Resonance frequency	f_R	0.5 V_{RMS}	32 kHz
Stiffness	k	120 V various load stiffness; preload 10 N	130 N/mm
Acceleration unipolar[2)] (see Fig. 5.)	a	20 g, single pulse sine wave, 200 Hz, 0 ... 120 V	17 · *g* (peak to peak) 7 · *g* (peak)
		100 g, single pulse sine wave, 200 Hz, 0 ... 120 V	13 · *g* (peak to peak) 7 · *g* (peak)
		500 g, single pulse sine wave, 200 Hz , 0 ... 120 V	3 · *g* (peak to peak) 1.2 · *g* (peak)
Acceleration bipolar[2)] (see Fig. 6.)	a	20 g, single pulse sine wave, 200 Hz, −20 ... 20 V	11 · *g* (peak to peak) 5.5 · *g* (peak)
		100 g, single pulse sine wave, 200 Hz, −20 ... 20 V	1.5 · *g* (peak to peak) 0.8 · *g* (peak)

1) Characterization performed with the support of AddHaptics Inc.

2) g is unit of measure of acceleration. 1 g is the acceleration due to gravity at the earth's surface 1 · g = 9.81 m/s².